

國立交通大學
機械工程研究所

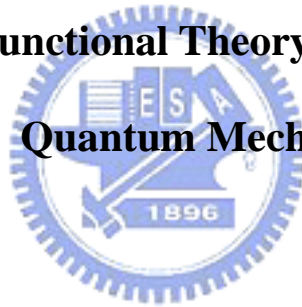
碩士論文

於量子力學中一個新密度函數理論之有限元素數值解初探

Preliminary Finite-Element Solution of a Self-consistent

Density Functional Theory Formulation in

Quantum Mechanics



研究生：陳永彬

指導教授：吳宗信 博士

中華民國九十三年七月

於量子力學中一個新密度函數理論之有限元素數值解初探

Preliminary Finite-Element Solution of a Self-consistent Density

Functional Theory Formulation in Quantum Mechanics

研究生：陳永彬

Student : Yung-Bin Chen

指導教授：吳宗信 博士

Advisor : Dr. Jong-Shinn Wu

國立交通大學

機械工程研究所

碩士論文

A Thesis

**Submitted to Institute of Mechanical Engineering Collage of
Engineering**

National Chiao Tung University

In Partial Fulfillment of the Requirements

for the degree of

Master of Science

In

Mechanical Engineering

July 2004

Hsinchu, Taiwan, Republic of China

中華民國九十三年七月

誌謝

首先感謝我的家人，父母親陳民生先生和洪素嬌女士全力的支持我唸書，讓我沒有顧慮的全心在學業上，以及弟弟陳伯煒在生活上的互相勉勵。

在交大的這兩年來，感謝吳宗信老師悉心教導，讓我無論是在學習過程中或是生活上都成長許多，在研究及做學問方面，因著老師不厭其煩的教導，而使我的能力成長許多，處理事情以及解決問題變得更有效率，並且也充實了我許多日常生活經驗，感謝老師這些日子以來的照顧。同時也感謝口試委員江進福教授、劉晉良教授和許正餘博士在口試時提供的寶貴意見，使得本論文更加充實，在此一併致謝。

實驗室的成員的感情融洽，使得我們在良好的學習環境學習，使得在學習過程中更有效率，同窗的情誼將永遠在我心中留下不可磨滅回憶。感謝學長許祐霖、邵雲龍、許國賢、曾坤樟、李允民、連又永、梁桂雄、許哲綱、吳明諭、及學姐周欣芸在研究上及生活上的教導及幫助，感謝同學吳俊賢、鄭淵文、吳志輝在學習上的相互切磋砥礪，以及學弟妹們生活上的幫助與鼓勵，使我這兩年的研究生生活非常充實且溫馨。

此外，感謝在交大這二年的生活中陪伴著我的各位好友。在這離別的季節裡，大家各奔前程，去追求偉大的夢想。希望大家在不久的將來，我們都能擁有屬於自己的一片天空。我會珍惜一路走來的種種回憶，願大家將來都能順利。

最後，再次獻上我最真摯的祝福，感謝在交大的每位師長、同學以及朋友們以及我最感謝的家人，由於你們的鼓勵與支持，才使我在求學的過程中能無憂無慮。真的，謝謝你們！

陳永彬 謹誌

甲申年七月于風城交大

於量子力學中一個新密度函數理論之有限元素數值解初探

學生：陳永彬

指導教授：吳宗信

國立交通大學機械工程研究所

摘要

在此研究中，我們利用有限元素法解一個由 Hsu[Hsu, 2003]推導出的新密度函數理論公式，此公式不同於 Kohn-Sham 方程式，其沒有因 exchange-correlation 項而另外做特別的假設來逼近問題。以有限元素法線性形狀函數的 Galerkin 殘差加權法來獲得特徵值線性代數方程式，再使用 Jacobi-Davidson 法求解特徵值方程式。發展一維和三維有限元素法的程式並和實驗或理論資料做比較。用來測試程式的問題包含一顆電子系統（如氫原子）沒有電子間的作用、兩顆電子系統（如類氫原子）和四顆電子系統（如類鈹原子）有電子間的作用。結果顯示一維和三維的程式所獲得的氫原子特徵狀態能量與實驗資料相當接近，對氫原子的穩態能量而言，其三維的程式尚在發展中，相關的結果希望能夠在論文口頭報告時呈現，另外由於三維有限元素法勁度矩陣的對角線優勢，三維程式的收斂速度遠快於一維程式。

Preliminary Finite-Element Solution of a Self-consistent Density

Functional Theory Formulation in Quantum Mechanics

Student : Yung-Bin Chen

Advisor : Dr. Jong-Shinn Wu

Institute of Mechanical Engineering

National Chiao Tung University

ABSTRACT

In the current study, we have used the finite element method (FEM) to solve a new formulation in density functional theory by Hsu [Hsu, 2003], in which, unlike Kohn-Sham equation, there is no exchange-correlation term, often requiring *ad hoc* assumption to close the problem. In this finite element method, Galerkin weighted residual method with linear shape function is used to obtain the eigenvalued linear algebra equations. Resulting eigenvalued equations are then solved using Jacobi-Davison method. Both 1-D and 3-D FEM codes are developed and compared with experimental or theoretical data wherever available. Benchmark test problems include one-electron system (e.g., hydrogen atom) without electron-electron interaction, two-electron system (e.g., helium-like atoms) and four-electron system (e.g., beryllium-like atoms) with electron-electron interactions. Results show that the eigenstate energies of hydrogen atom obtained by both 1-D and 3-D codes approach

the experimental data. The ground state energy of helium atom using 3-D FEM code is still in progress. Related results hopefully will be presented in the oral examination of my thesis. In addition, convergence rate in 3-D code is generally much faster than that in 1-D code due to the diagonal dominance in the stiffness matrix of 3-D FEM.



TABLE OF CONTENTS

摘要.....	I
ABSTRACT.....	II
TABLE OF CONTENTS.....	IV
LIST OF TABLES.....	VI
LIST OF FIGURES	VII
CHAPTER 1 INTRODUCTION.....	1
1.1 Motivation.....	1
1.1.1 Multiscale Simulation in Materials Processing.....	1
1.2 Background.....	2
1.3 Literature Surveys.....	4
1.3.1 Theoretical Development.....	4
1.3.1.1 Schrödinger equation.....	4
1.3.1.2 Hartree-Fock Theory.....	4
1.3.1.3 Hohenberg & Kohn Theorem.....	5
1.3.1.4 Kohn-Sham Equations.....	5
1.3.1.5 A New Density Functional Theory Formulation.....	6
1.3.2 Numerical Methods.....	6
1.3.2.1 Orbital-type method.....	7
1.3.2.2 Real-space method.....	7
1.4 Objectives of the Thesis.....	9
CHAPTER 2 DENSITY FUNCTIONAL THEORY	11
2.1 Ab-initio Methods.....	11
2.1.1 Schrödinger Equation.....	11
2.1.2 Hartree Theory.....	12
2.1.3 Hartree-Fock Theory.....	14
2.1.4 Exchange-Correlation Energy.....	15
2.1.5 Hohenberg & Kohn Theorem.....	17
2.1.6 Kohn-Sham Equations.....	19
2.2 Approximation to the Exchange-correlation Function.....	21
2.2.1 Local Density Approximation (LDA).....	21
2.2.2 Generalized Gradient Approximation (GGA).....	22
2.3 New Density Functional Theory Formulation.....	22
CHAPTER 3 NUMERICAL METHOD	25

3.1	Finite Element Method (FEM).....	26
3.1.1	One-dimensional FEDFT Program.....	28
3.1.2	Three-dimensional FEDFT Program.....	30
3.2	Jacobi-Davidson Method.....	33
CHAPTER 4	RESULTS AND DISCUSSIONS.....	36
4.1	Elements Construction.....	36
4.1.1	One-dimensional Elements.....	36
4.1.2	Three-dimensional Elements.....	37
4.2	One-dimensional FEDFT.....	37
4.3	Three-dimensional FEDFT.....	39
CHAPTER 5	CONCLUSIONS.....	42
CHAPTER 6	FUTURE WORKS.....	44
REFERENCES.....		45
APPENDIX A.....		47
APPENDIX B.....		53



LIST OF TABLES

Table 4.1	The radial domain data of all models for one-dimensional FEDFT in this research. Cutoff radius is in units of Bohr radius.	60
Table 4.2	The computational domain data of all models for three-dimensional FEDFT in this research. Cutoff radius is in units of Bohr radius.	61
Table 4.3	Hydrogen atom. The energies of the electron obtained by one-dimensional FEDFT program compared with experiment. Energy is in units of eV.	62
Table 4.4	Helium-like atoms. The energies of the electron obtained by one-dimensional FEDFT program compared with experimental ones and numerical ones obtained by Hsu. Energy is in units of eV.	63
Table 4.5	Beryllium-like atoms. The energies of the electron obtained by one-dimensional FEDFT program compared with experimental ones and numerical ones obtained by Hsu. Energy is in units of eV.	64
Table 4.6	Hydrogen atom. The energies of the electron obtained by three-dimensional FEDFT program compared with experimental ones and numerical ones obtained by one-dimensional FEDFT. Energy is in units of eV. 65	65
Table 4.7	Helium atom. The energies of the electron obtained by three-dimensional FEDFT program compared with experimental ones and numerical ones obtained by Hsu and one-dimensional FEDFT. Energy is in units of eV.	66
Table B.1	Numerical integration formula of Gauss Quadrature for tetrahedral element [Zienkiewicz and Taylor, 2000].	67

LIST OF FIGURES

Fig. 1.1 Sketch of the multiscale and physical processes in a DC-magnetron sputtering chamber.	68
Fig. 1.2 The analysis of vapor deposition spans both a wide length and time scale. Overlapping modeling methods are beginning to allow an increasingly rigorous multiscale treatment [Ohno et al., 1999; Olson, 1997].	69
Fig. 1.3 The publications about DFT [Friedrich].	70
Fig. 1.4 STOs & GTOs [Friedrich]	71
Fig. 2.1 The proof of Hohenberg & Kohn second theorem	72
Fig. 3.1 The flow chart of the FEDFT.	73
Fig. 3.2 The flow chart of the J-D solver.	74
Fig. 4.1 One-dimensional meshes with 4 elements and 5 nodes.	75
Fig. 4.2 The tetrahedral element.	76
Fig. 4.3 The surface meshes of three-dimensional computational domain with different view points. ($r=10$ Bohr radii, $\theta=30^\circ$, $\varphi=30^\circ$)	77
Fig. 4.4 The probabilities of finding the electron in a hydrogen atom at a distance between r and $r + dr$ from the nucleus for the 1s and 2s state obtained by one-dimensional FEDFT compared with exact solutions.	78
Fig. 4.5 The probabilities of finding the electron in a He at a distance between r and $r + dr$ from the nucleus for the 1s and 2s state obtained by one-dimensional FEDFT.	79
Fig. 4.6 The probabilities of finding the electron in a Li^+ at a distance between r and $r + dr$ from the nucleus for the 1s and 2s state obtained by one-dimensional FEDFT.	80
Fig. 4.7 The probabilities of finding the electron in a Be^{+2} at a distance between r and $r + dr$ from the nucleus for the 1s and 2s state obtained by one-dimensional FEDFT.	81
Fig. 4.8 The probabilities of finding the electron in a B^{+3} at a distance between r and $r + dr$ from the nucleus for the 1s and 2s state obtained by one-dimensional FEDFT.	82
Fig. 4.9 The probabilities of finding the electron in a C^{+4} at a distance between r and $r + dr$ from the nucleus for the 1s and 2s state obtained by one-dimensional FEDFT.	83
Fig. 4.10 The probabilities of finding the electron in helium-like atoms at a distance between r and $r + dr$ from the nucleus for the 1s state obtained by one-dimensional FEDFT.	84
Fig. 4.11 The probabilities of finding the electron in helium-like atoms at a distance	

between r and $r + dr$ from the nucleus for the 2s state obtained by one-dimensional FEDFT.....	85
Fig. 4.12 The probabilities of finding the electron in a Be at a distance between r and $r + dr$ from the nucleus for the 1s and 2s state obtained by one-dimensional FEDFT.....	86
Fig. 4.13 The probabilities of finding the electron in a B^+ at a distance between r and $r + dr$ from the nucleus for the 1s and 2s state obtained by one-dimensional FEDFT.....	87
Fig. 4.14 The probabilities of finding the electron in a C^{+2} at a distance between r and $r + dr$ from the nucleus for the 1s and 2s state obtained by one-dimensional FEDFT.....	88
Fig. 4.15 The probabilities of finding the electron in beryllium-like atoms at a distance between r and $r + dr$ from the nucleus for the 1s and 2s state obtained by one-dimensional FEDFT.....	89
Fig. 4.16 Photographic representation of the electron probability-density distribution for 1s and 2s states. These may be regard as sectional views of the distribution in a plane containing the polar axis, which is vertical and in the plane of the paper [Arthur, 1995].	90
Fig. 4.17 The 1s state convergence of residual with iterations for hydrogen atom by one-dimensional and three-dimensional FEDFT.	91
Fig. 4.18 The 2s state convergence of residual with iterations for hydrogen atom by one-dimensional and three-dimensional FEDFT.	92
Fig. 4.19 The probabilities of finding the electron in a hydrogen atom at a distance between r and $r + dr$ from the nucleus for the 1s and 2s state obtained by three-dimensional FEDFT compared with exact solutions.....	93
Fig. 4.20 The probability of finding the electron in a helium atom at a distance between r and $r + dr$ from the nucleus for the 1s state obtained by three-dimensional FEDFT compared with one-dimensional FEDFT.....	94
Fig. B.1 The coordinates of point P described by four edge nodes in the tetrahedral element [Zienkiewicz and Taylor, 2000].	95

CHAPTER 1 INTRODUCTION

1.1 Motivation

1.1.1 Multiscale Simulation in Materials Processing

Vapor deposition (Fig. 1.1) is a multiscale process in the sense that growth of the film occurs in a reactor whose dimensions are of $O(1\text{m})$ for a time of $O(10^2\text{s})$, while the atomic assembly events involve length scales of $O(10^{-10}\text{m})$ with time scales in the pico- to micro-second region. In fact, atomic assembly is more fundamentally determined by the making and breaking of chemical bonds which is described by the wave functions of bonding electrons with length and time scales of $O(10^{-13}\text{m}$ and $10^{-16}\text{s})$, respectively. Vapor deposition is not unique in this respect — all of materials science confronts a similar issue and many approaches have evolved for treating it [Ohno *et al.*, 1999; Olson, 1997].

The ability to design processes for the growth of an atomic scale structure is critically tied to our ability to connect models with very disparate time and length scales. This ranges from the use of quantum mechanics to describe atomic binding to computational fluid dynamics (CFD) or direct simulation Monte Carlo (DSMC) [Bird, 1994] to account for complex flow fields, thermal gradients and reaction

environments in the deposition chamber. This modeling hierarchy is summarized in Fig. 1.2. Some state-of-the-art modeling and simulation tools such as density functional theory (DFT), molecular dynamics (MD), kinetic Monte Carlo (kMC) and CFD when used alone enable analysis of only a part of a synthesis process. Among these, kMC method can be used to study the slow thermal diffusion of the deposited atoms/molecules on the substrate surface, which is important for predicting the correct morphology of the material structure. Energy barrier for atom jump at various atomic configurations on the substrate surface is required in the kMC method. However, it is very hard to obtain the data from experiment due to the difficulty of manipulating atom by atom precisely. Quantum computation considering large-scale atomic structure using DFT is the most possible and correct method to derive the data [Wadley *et al.*, 2001].

1.2 Background

To describe completely the quantum mechanical behavior of electrons in solids it is strictly necessary to calculate the many-electron wave function for the system. In principle this may be obtained from the time-independent Schrödinger equation, but in practice the potential experienced by each electron is dictated by the behavior of all the other electrons in the solid. To solve the Schrödinger equation directly for all these

electrons would thus require us to solve a system of around 10^{23} simultaneous differential equations. Such a calculation is beyond the capabilities of computers nowadays, and is likely to remain so for the foreseeable future. Evidently, we must involve some approximations to render the problem soluble albeit tricky. Here we have our simplest definition of DFT: A method of obtaining an approximate solution to the Schrödinger equation of a many-body system.

For the past 30 years density functional theory has been the dominant method for the quantum mechanical simulation of periodic systems. In recent years it has also been adopted by quantum chemists and is now very widely used for the simulation of energy surfaces in molecules (Fig. 1.3).

Either Schrödinger equation or DFT formulation are the eigenvalue problems. In the current thesis, we use the finite element method (FEM) to derive the matrix equation from DFT formulation and then use some efficient matrix solver to solve the eigenvalue (energy) and corresponding eigenvector. Advantages of using FEM for solving the DFT formulation include easier parallel implementation employing domain decomposition [Wu and Hsu, 2004] and possible mesh refinement in the regions where solution changes rapidly [Wu *et al.*, 2004].

1.3 Literature Surveys

1.3.1 Theoretical Development

1.3.1.1 Schrödinger equation

The foundation of the theory of electronic structure of matter is the non-relativistic Schrödinger equation for the many-electron wave function Ψ [Schrödinger, 1926]. The much heavier nuclei are considered as fixed in space by the Born-Oppenheimer approximation, so the wave function Ψ depends on the position and spins of the N electrons [Michael, 2000].

1.3.1.2 Hartree-Fock Theory

Within Hartree-Fock theory one assumes the wave function of the N particle (electron) system to be an anti-symmetrized product of one particle (electron) functions [Markus, 2002]. Moreover, the HF is an approximation, as it does not account for dynamic correlation due to the rigid form of single determinant wave function. To account for dynamic correlation, one has to go to correlated methods, which use multi-determinant wave functions, and these scales as fifth, or even greater powers with the size of a system [Jan, 1996].

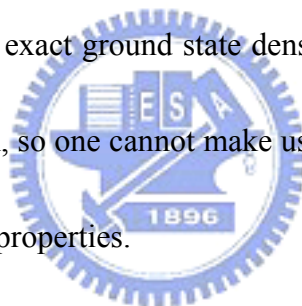
The calculation of the many-body wave function of a system of interacting electrons is a formidable task, which can only be carried out – and is only

meaningful – for systems with a few tens of electrons [Kohn, 1999]. Its observables for larger systems are to be determined; the calculation of the many-body wave functions has to be avoided due to the seemingly formidable computational difficulty.

1.3.1.3 Hohenberg & Kohn Theorem

In the year 1964 Hohenberg and Kohn published a paper in Physical Review, where they stated two fundamental theorems, which gave birth to modern density functional theory, an alternative approach to deal with the many body problem in electronic structure theory [Hohenberg and Kohn, 1964].

Up till now, both the exact ground state density as well as the Hohenberg-Kohn functional is still unknown, so one cannot make use of the Hohenberg-Kohn theorems to calculate the molecular properties.



1.3.1.4 Kohn-Sham Equations

Kohn and Sham introduced a fictitious system of N non-interacting electrons to be described by a single determinant wave function in N “orbits” [Kohn and Sham, 1965]. The construction of the density explicitly from a set of orbits ensures that it is legal – it can be constructed from an asymmetric wave function. Due to the second part of the H&K theorem, namely that the total energy is minimized by the true ground-state density, the variational principle can now be utilized. With the standard functional derivatives and the additional definition of the so-called

exchange-correlation potential. The exchange-correlation functional, ϵ_{xc} , which is simply the sum of the error made in using a non-interacting kinetic energy and the error made in treating the electron-electron interaction classically [Harrison].

All that remains now is the question what to do with the ϵ_{xc} , without which one cannot do any practical calculations. As mentioned above, this term has to tread on an approximate manner. Although there are many different functions available, almost all of them are derived from the electron density of a *uniform electron gas*, which can be calculated by means of statistical thermodynamics.

1.3.1.5 A New Density Functional Theory Formulation

In a recent paper, a generic derivation from cluster expansion results in a new DFT formulation without the exchange-correlation term that makes the computation much traceable in physics without *ad hoc* assumption as mentioned in the above [Hsu, 2003].

1.3.2 Numerical Methods

In the past, numerical methods for solving DFT formulation can be divided into two categories. One is orbital-type method and the other is real-space method. The former includes computations using slater-type orbitals (STOs), Gaussian-type orbitals (GTOs) and plane waves, while the latter is the real-space method that can be

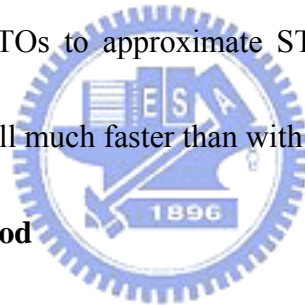
loosely categorized as finite differences (FD), finite elements (FE), and wavelets.

1.3.2.1 Orbital-type method

Linear combinations of analytical functions $\varphi_i(r) = \sum_j c_{i\kappa} \chi_\kappa(r)$

- Plane Waves, $\chi_\kappa(r) = \exp(ik_\kappa r)$
- Slater Type Orbitals, $\chi_\kappa(r) = x^{k_\kappa} y^{l_\kappa} z^{m_\kappa} \cdot \exp(-\zeta_\kappa r)$, whose shape close to true orbits (hydrogen atom) but evaluation of integrals is expensive.
- Gaussian Type Orbitals, $\chi_\kappa(r) = x^{k_\kappa} y^{l_\kappa} z^{m_\kappa} \cdot \exp(-\zeta_\kappa r^2)$, whose evaluation of integrals cheap but different from true orbital shape.

Linear combination of GTOs to approximate STOs that is 1 STO \approx 3 GTOs, but analytical integration is still much faster than with STOs (Fig. 1.4).



1.3.2.2 Real-space method

Real-space methods can loosely be categorized as one of three types: finite differences (FD), finite elements (FE), or wavelets. All three lead to structured, very sparse matrix representations of the underlying differential equations on meshes in real space. Applications of wavelets in electronic structure calculations have been thoroughly reviewed recently [Arias, 1999]. As implied in the title, the primary focus is on calculations in density functional theory (DFT); real-space methods are in no way limited to DFT, but since DFT calculations comprise a dominant theme in modern electrostatics and electronic structure, the discussion here will mainly be

restricted to this particular theoretical approach.

The early development of FD and FE methods for solving partial differential equations stemmed from engineering problems involving complex geometries, where analytical approaches were not possible [Strang and Fix, 1973]. Example applications include structural mechanics and fluid dynamics in complicated geometries. However, even in the early days of quantum mechanics, attention was paid to FD numerical solutions of the Schrödinger equation [Kimball and Shortley, 1934; Pauling and Wilson, 1935].

Real-space calculations are performed on meshes; these meshes can be as simple as Cartesian grids or can be constructed to conform to the more demanding geometries arising in many applications. Finite-difference representations are most commonly constructed on regular Cartesian grids. They result from a Taylor series expansion of the desired function about the grid points. The advantages of FD methods lie in the simplicity of the representation and resulting ease of implementation in efficient solvers. Disadvantages are that the theory is not variational, and it is difficult to construct meshes flexible enough to conform to the physical geometry of many problems. Finite-element methods, on the other hand, have the advantages of significantly greater flexibility in the construction of the mesh and an underlying variational-type formulation. Other advantages include easier

parallel implementation using domain decomposition and possible mesh refinement in regions where solution changes rapidly, as mentioned earlier. However, the cost of the flexibility is an increase in complexity and more difficulty in the implementation of multiscale or related solution methods [Thomas, 2000].

1.4 Objectives of the Thesis

It is very attractive that this new DFT formulation can be solved without the uncertainty caused by the exchange-correlation term in principle. However, this DFT formulation is a typical eigenvalue problem, which is in principle more difficult to solve than a boundary-value problem from the numerical viewpoint. The design of the numerical scheme has to consider the future applications to system having a large numbers of electrons, which requires tremendous computing resources. In addition, the probability of electrons near the immobile ions (nucleus) often presents very large variations. Thus, in the current study we solve this new DFT formulation using finite element method, in which the advantages can be taken in the future for *mesh refinement* and *parallelization* using graph-partitioning technique (or domain decomposition).

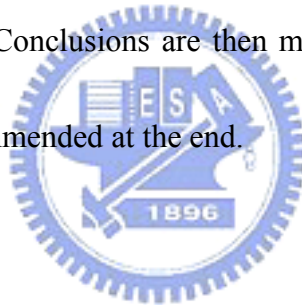
Therefore, the objectives of the current study are summarized as follows.

1. To complete both 1-D and 3-D FE programs for solving the new DFT

formulation.

2. To apply the two programs to compute simple atomic (1 nucleus) systems, such as hydrogen atom (1 electron), helium-like atoms (2 electrons) and beryllium-like atoms (4 electrons).
3. To verify and compare the performance of 1-D and 3-D FE programs by comparing with available experimental data.

The thesis begins with descriptions of the FE method appropriate in the discreteness of 1-D and 3-D problems. Results of 1-D and 3-D computations are presented and discussed. Conclusions are then made in turn. Future development in this direction is also recommended at the end.



CHAPTER 2 DENSITY FUNCTIONAL THEORY

2.1 Ab-initio Methods

2.1.1 Schrödinger Equation

The initial work on Density Functional Theory (DFT) was reported in two publications: the first with Pierre Hohenberg in 1964 and the next with Lu J. Sham in 1965. This was almost 40 years after E. Schrödinger [Schrödinger, 1926] published his first epoch-making paper marking the beginning of wave-mechanics.


$$\text{Schrödinger equation: } \left(-\frac{1}{2} \sum_i \nabla_i^2 - \sum_i \sum_a \frac{Z_a}{|r_i - R_a|} + \sum_{i,j} \frac{1}{|r_i - r_j|} \right) |\Psi\rangle = E |\Psi\rangle \quad (2.1)$$

Where r_i, r_j are the positions of the electrons and R_a, Z_a are the positions and atomic numbers of the nuclei; and E is the energy. We will be primarily concerned with the calculation of the ground state energy of a collection of atoms. The energy may be computed by solution of the Schrödinger equation – which, in the time independent, non-relativistic, Born-Oppenheimer approximation is

$$H\Psi(r_1, r_2, \dots, r_N) = E\Psi(r_1, r_2, \dots, r_N) \quad (2.2)$$

The wave function Ψ depends on the position and spins of the N electrons. The Hamiltonian operator, H , consists of a sum of three terms: the kinetic energy, the interaction with the external potential (V_{ext}) and the electron-electron interaction (V_{ee}).

That is

$$H = -\frac{1}{2} \sum_i^N \nabla_i^2 + V_{ext} + \sum_{i < j}^N \frac{1}{|r_i - r_j|} \quad (2.3)$$

In materials simulation the external potential of interest is simply the interaction of the electrons with the atomic nuclei

$$V_{ext} = -\sum_i \sum_a \frac{Z_a}{|r_i - R_a|} \quad (2.4)$$

Note that in order to simplify the notation and to focus the discussion on the main features of DFT the spin coordinate is omitted here and throughout this article. The lowest energy eigenvalue, E_0 , is the ground state energy and the probability density of finding an electron with any particular set of coordinates $\{\mathbf{r}_i\}$ is $|\Psi_0|^2$.

2.1.2 Hartree Theory



One of the earliest attempts to solve the problem was made by Hartree. He simplified the problem by making an assumption about the form of the many-electron wave function, namely that it was just the product of a set of single-electron wave functions. Having made this assumption it was possible to proceed using the variational principle.

In fact, for an N -electron system there are N equations for each of the N single-electron wave functions, which made up the many-electron product wave function [Stephen, 1997]. These equations turned out to look very much like the

time-independent Schrödinger equation, except the potential (the Hartree potential) was no longer coupled to the individual motions of all the other electrons, but instead depended simply upon the time-averaged electron distribution of the system. This important fact meant that it was possible to treat each electron separately as a single-particle.

$$\Psi = \prod_{i=1}^N \varphi_i(\vec{r}_i) \quad (2.5)$$

where the φ_i are orthonormal. Consequently the Hartree approximation allows us to calculate approximate single-particle wave functions for the electrons in crystals, and hence calculate other related properties. Unfortunately, the Hartree approximation does not provide us with particularly good results.

The central failing of the Hartree approximation is that it does not recognize the Pauli exclusion principle. The true many-body wave function must vanish whenever two electrons occupy the same position, but the Hartree wave function cannot have this property. Mathematically, the Pauli exclusion principle can be accounted for by ensuring that the wave function of a set of identical fermions is anti-symmetric under exchange of any pair of particles. That is to say that the process of swapping any one of the fermions for any other of the fermions should leave the wave function unaltered except for a change of sign. Any wave function possessing that property will tend to zero (indicating zero probability) as any pair of fermions with the same quantum

numbers approaches each other. The Hartree product wave function is symmetric rather than anti-symmetric, so the Hartree approach effectively ignores the Pauli exclusion principle!

2.1.3 Hartree-Fock Theory

The Hartree-Fock approach is an improvement over the Hartree theory in that the many-electron wave function is specially constructed out of single-electron wave functions in such a way as to be anti-symmetric. The wave function has to be much more complicated than the Hartree product wave function, but it can be written in a compact way as a so-called Slater determinant (for those who know what a determinant is).

$$\Psi_{HF} = \frac{1}{\sqrt{N!}} \det[\varphi_1 \varphi_2 \varphi_3 \cdots \varphi_N] \quad (2.6)$$

$$\Psi = \frac{1}{\sqrt{N!}} \begin{vmatrix} \varphi_1(r_1) & \varphi_1(r_2) & \cdots & \varphi_1(r_N) \\ \varphi_2(r_1) & \varphi_2(r_2) & \cdots & \varphi_2(r_N) \\ \vdots & \vdots & & \vdots \\ \varphi_N(r_1) & \varphi_N(r_2) & \cdots & \varphi_N(r_N) \end{vmatrix} \quad (2.7)$$

Where the variables r_i include the coordinates of space and spin. This simple ansatz for the wave function Ψ captures much of the physics required for accurate solutions of the Hamiltonian. Most importantly, the wave function is anti-symmetric with respect to an interchange of any two-electron positions.

$$\Psi(r_1, r_2, \cdots, r_i, r_{i+1}, \cdots, r_N) = -\Psi(r_1, r_2, \cdots, r_{i+1}, r_i, \cdots, r_N) \quad (2.8)$$

Starting from this assumption it is once again possible to derive the Hamiltonian equation for the system through the variational principle. Just as before, this results in a simple equation for each single-electron wave function. However, this time in addition to the Hartree potential (which described the direct Coulomb interaction between an electron and the average electron distribution) there is now a second type of potential influencing the electrons, namely the so-called exchange potential. The exchange potential arises as a direct consequence of including the Pauli exclusion principle through the use of an anti-symmetric wave function.

Notably, the exchange potential contributes a binding energy for electrons in a neutral uniform system, so correcting one of the major failings of the Hartree theory. However, in calculating many other properties the Hartree-Fock approach is actually worse than the Hartree approach.

2.1.4 Exchange-Correlation Energy

The reason the Hartree-Fock theory gives worse answers than the Hartree theory is simply that there is another piece of physics, which we are still ignoring. To some extent it cancels out with the exchange effect and so when we use the Hartree approach (i.e. we ignore both effects) we obtain reasonable results. On the other hand the Hartree-Fock approach includes the exchange effect but ignores the other effect,

which balances it somewhat, completely. This new effect is the electrostatic correlation of electrons.

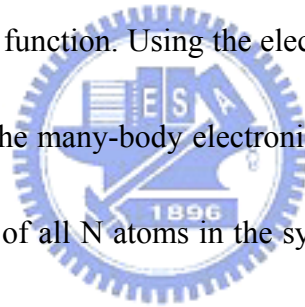
Ignoring the Pauli exclusion principle generated exchange hole for the moment, we can also visualize a second type of hole in the electron distribution caused by simple electrostatic processes. If we consider the region immediately surrounding any electron (spin is now immaterial) then we should expect to see fewer electrons than the average, simply because of their electrostatic repulsion. Consequently each electron is surrounded by an electron-depleted region that known either the Coulomb hole (because of its origin in the electrostatic interaction) or the correlation hole (because of it origin in the correlated motion of the electrons). Just as in the case of the exchange hole the electron-depleted region is slightly positively charged. The effect of the correlation hole is twofold. Thus any other interaction effects, such as exchange, will tend to be reduced by the correlation hole [Stephen, 1997].

Clearly we can now see why the Hartree-Fock approach fails for solids: firstly the exchange interaction should be screened by the correlation hole rather than acting in full, and secondly the binding between the correlation hole and electron has been ignored. At this point, the Hartree-Fock approach gives quite creditable results for small molecules. This is because there are far fewer electrons involved than in a solid, and so correlation effects are minimal compared to exchange effects.

2.1.5 Hohenberg & Kohn Theorem

The discussion above has established that direct solution of the Schrödinger equation is not currently feasible for systems of interest in condensed matter science – this is a major motivation for the development and use of density functional theory.

DFT is based upon a fundamental observation that the total energy of an assembly of atoms is a function of the total electron charge density [Hohenberg and Kohn, 1964], which is a function of space and time. The electron density is used in DFT as the fundamental property unlike Hartree-Fock theory, which deals directly with the many-body wave function. Using the electron density significantly speeds up the calculation. Whereas the many-body electronic wave function is a function of $3N$ variables (the coordinates of all N atoms in the system) the electron density is only a function of x, y, z only three variables.



In 1964 Hohenberg and Kohn proved the two theorems:

1. For a non-degenerate ground state Ψ of the system the external potential $V_{\text{ext}}(r)$ is determined, within a trivial additive constant, as a functional of the electronic density $n(r)$.
2. Given an external potential $V_{\text{ext}}(r)$, the correct ground-state density $n(r)$ minimizes the ground-state energy E_0 , which is a functional uniquely determined by $n(r)$. It holds,

$$E_0 \leq E_v[\tilde{n}] \quad (2.9)$$

where $\tilde{n}(r)$ is any trial density fulfilling $\tilde{n}(r) \geq 0$ and $\int d^3r \tilde{n}(r) = N$, N being the number of electrons in the system.

They considered the ground state of the system to be defined by that electron density distribution which minimizes the total energy. Furthermore, they showed that all other ground state properties of the system (e.g. lattice constant, cohesive energy, etc) are functional of the ground state electron density. That is, that once the ground state electron density is known all other ground state properties follow (in principle, at least).



The theorem – which has a remarkable short proof (Fig. 2.1) – guarantees the existence of an energy functional $E[n]$ that reaches its minimum for the correct density $n(r)$ yet gives no explicit prescription for its construction [Stephen, 1997]. In order to determine $E[n]$ it is useful to separate the various known contributions to the total energy, like $T_s[n]$, the kinetic energy of a non-interacting electron gas, $E_{ext}[n]$, the classical Coulomb energy of the electrons moving in the external potential $V_{ext}(r)$, and $E_{Coul}[n]$, the classical energy due to the mutual Coulomb interaction of the electrons:

$$E[n(r)] = T_s[n(r)] + E_{ext}[n(r)] + E_{Coul}[n(r)] + E_{xc}[n(r)] \quad (2.10)$$

The last term $E_{xc}[n]$ contains the quantum-mechanical exchange and correlation energy and – in principle – the difference between the true kinetic energy, $T[n]$, and

$T_s[n]$, the kinetic energy of the gas of non-interacting Kohn-Sham electrons. But since this difference is very small it is typically neglected.

2.1.6 Kohn-Sham Equations

Due to the second part of the H&K theorem, namely that the total energy is minimized by the true ground-state density, the variational principle can now be utilized. With the standard functional derivatives and the additional definition of the so-called exchange-correlation potential,

$$v_{xc}(r) = \frac{\delta E_{xc}[\tilde{n}(r)]}{\delta \tilde{n}(r)} \quad (2.11)$$

the following set of equations can be derived

$$\left[-\frac{1}{2} \nabla^2 + v_{eff}(r) \right] \varphi_i(r) = \varepsilon_i \varphi_i(r) \quad (2.12)$$

where the effective potential – as a functional of the electronic density – is given by

$$v_{eff} = v_{eff}[n(r)] = v_{ext}(r) + \int dr' \frac{n(r')}{|r-r'|} + v_{xc}[n(r)] \quad (2.13)$$

and the electronic density as

$$n(r) = \sum_{i=1}^N |\varphi_i(r)|^2 \quad (2.14)$$

The set of equations (2.12) to (2.14) are the famous Kohn-Sham (KS) equations. They have to be solved self-consistently, i.e., starting from some initial density a potential $v_{eff}[n(r)]$ is obtained for which the Eq. (2.12) are solved and a new electronic density Eq. (2.14) is determined. From the new density an updated effective potential can be

calculated and this process is repeated until self-consistency is reached, i.e., until the new electronic density equals the previous one [Schöne].

In fact, the K-S equations give an exact description of the many-electron system since up to this point no approximations have been made. Nevertheless, the method has reasonable precision from the past experience. First-principle DFT methods can currently predict binding energies to within a tenth of an electron volt and bond lengths to within 0.02 Å. It is becoming relatively straightforward to use this method to analyze the kinetics of relevant surface processes, including adsorption, chemical reaction and diffusion. However, there exists an exchange-correlation functional E_{xc} due to electrons in general DFT, which often requires some *ad hoc* assumptions (e.g., local density approximation (LDA) assuming uniform electron gas, [Seminario and Politzer, 1995]) to close the problem.

The success of the density functional theory (DFT) in reproducing measurable physical quantities of many-electron systems is rather remarkable, and may be attributed to the very fact that in the configuration space where exists a density distribution that is unique, and corresponding to the lowest energy state, no matter how complex and populous the system might be. There are, however, physical properties that will require the phase space information, at the minimum the pair correlation in order to quantify the electron-electron interaction energy.

2.2 Approximation to the Exchange-correlation Function

The generation of approximations for E_{xc} has led to a large and still rapidly expanding field of research. There are now many different flavors of functionals available which are more or less appropriate for any particular study.

2.2.1 Local Density Approximation (LDA)

The simplest, and at the same time remarkably serviceable, approximation for $E_{xc}[n(r)]$ is the so-called local density approximation (LDA). It is assumed that the density of an inhomogeneous system can be locally described by a homogeneous electron gas [Hohenberg and Kohn, 1964]. A homogeneous electron gas is fully specified by its electronic particle density n , which is often expressed in terms of the corresponding Wigner-Seitz radius r_s ,

$$r_s = \left(\frac{3}{4\pi n} \right)^{1/3} \quad (2.15)$$

Within the LDA the functional for the exchange-correlation energy, E_{xc} , can be written as

$$E_{xc}[n] = \int d^3r [n(r)\varepsilon_{xc}[n(r)]] \quad (2.16)$$

where ε_{xc} is the exchange-correlation energy per particle of a homogeneous electron gas of density n . In the next step, the exchange-correlation potential is split into its exchange part v_x and a correlation part v_c ,

$$v_{xc}(r_s) = v_x(r_s) + v_c(r_s) \quad (2.17)$$

The local density approximation can be considered to be the zeroth order approximation to the semi-classical expansion of the density matrix in terms of the density and its derivatives [Dreizler and Gross, 1990].

2.2.2 Generalized Gradient Approximation (GGA)

In the generalized gradient approximation (GGA) a functional form is adopted which ensures the normalization condition and that the exchange hole is negative definite [Perdew and Wang, 1986]. This leads to an energy functional that depends on both the density and its gradient but retains the analytic properties of the exchange correlation hole inherent in the LDA.

The typical form for a GGA functional is:

$$E_{xc} = \int d^3r [n(r)\varepsilon_{xc}(n(r), \nabla n(r))] \quad (2.18)$$

The GGA improves significantly on the LDA's description of the binding energy of molecules – it was this feature which led to the very wide spread acceptance of DFT in the chemistry community during the early 1990's.

2.3 New Density Functional Theory Formulation

In a recent paper [Hsu, 2003], a generic derivation from cluster expansion results in a new DFT formulation (Eq. (2.21) as follows) without the exchange-correlation

term that makes the computation potentially much traceable in physics itself without any *ad hoc* assumptions. It was derived from the Schrödinger equation and reached a different form from the other DFT formulation. The wave function Ψ is chosen as the product of a single-electron wave function Φ , and an N -body correlation function,

$$\Psi(\Gamma) = \prod_{i=1}^N \Phi(r_i) U(\Gamma) \quad (2.19)$$

Γ is the N -particle phase space point equivalent to the expression (r_1, r_2, \dots, r_n) . The exchange symmetry is imposed on U and on the indistinguishable particles so that each electron is described by the same Φ . This gives the density function as follows:

$$n(r) = \int \prod_{i=2}^N d\tau_i |\Phi(r_i)|^2 |U(r_1, r_2, \dots, r_N) \Phi(r)|^2 \equiv |\Psi_0(r)|^2 \quad (2.20)$$

where the index starting from $i=2$ is chosen for convenience by imposing the exchange symmetry, and $d\tau_i$ is the volume element of i th particle. The last derived equation is

$$\varepsilon \Psi_0(\bar{r}) = -\frac{1}{2} \nabla^2 \Psi_0(\bar{r}) - \sum_I \frac{Z_I}{|\bar{r} - \bar{R}_I|} \Psi_0(\bar{r}) + \frac{1}{2} (N-1) \Psi_0(\bar{r}) \left\langle \frac{1}{|\bar{r} - \bar{r}'|} \right\rangle \quad (2.21a)$$

where

$$\left\langle \frac{1}{|r - r'|} \right\rangle = \left\{ \int d^3 r' |\Psi_0(r')|^2 / |r - r'| \right\} / \int d^3 r' |\Psi_0(r')|^2 \quad (2.21b)$$

The subscript, I , refers to the immobile ion with charge Z_I and N represents the number of electrons. This equation differs from the conventional DFT in several aspects. The usual exchange-correlation function disappears in this new formulation,

while the electron-electron interaction differs by a factor $\frac{1}{2}(N-1)$. The derivation of the density functional theory (DFT) from the cluster expansion corrects the spurious self-interaction energy in the ‘classical’ DFT, admits the excited states, and has a self-consistent exchange correlation effect.



CHAPTER 3 NUMERICAL METHOD

The early development of FD and FE methods for solving partial differential equations stemmed from engineering problems involving complex geometries, where analytical approaches were not possible [Strang and Fix, 1973]. Example applications include structural mechanics and fluid dynamics in complicated geometries. However, even in the early days of quantum mechanics, attention was paid to FD numerical solutions of the Schrödinger equation [Kimball and Shortley, 1934, 10].

Real-space calculations [Thomas, 2000] are performed on meshes; these meshes can be as simple as Cartesian grids or can be constructed to conform to the more demanding geometries arising in many applications. Finite-difference representations are most commonly constructed on regular Cartesian grids. They result from a Taylor series expansion of the desired function about the grid points. The advantages of FD methods lie in the simplicity of the representation and resulting ease of implementation in efficient solvers. Disadvantages are that the theory is not variational, and it is difficult to construct meshes flexible enough to conform to the physical geometry of many problems. Finite-element methods, on the other hand, have the advantages of significantly greater flexibility in the construction of the mesh and an underlying variational formulation. In addition, parallel implementation using

domain decomposition, combining with adaptive mesh h-refinement, in FE methods due to unstructured mesh is rather straightforward by the use of graph-partitioning technique. The cost of these flexibilities may be an increase in complexity and more difficulty in the implementation.

3.1 Finite Element Method (FEM)

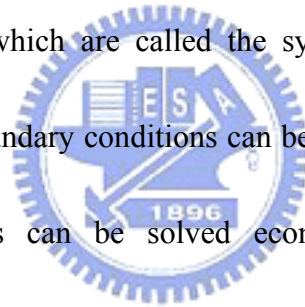
We begin with an introduction of the FEM that identifies the broad context of the subject [Burnett, 1987]:

The FEM is the computer-aid mathematical technique for obtaining approximate numerical solution to the abstract of calculus that predict the response of physical system subjected to the external influences.

Such problems arise in many areas of engineering, science, and applied mathematics. Applications to date have occurred principally in the areas of solid mechanics, heat transfer, fluid mechanics, and electromagnetism. New areas of application are continually being discovered, recent ones include solid-state physics and quantum mechanics.

The salient features in FEM include the following:

1. The domain is divided into smaller regions called elements. Adjacent elements touch without overlapping, and there are no gaps between the elements. The shapes of the elements are intentionally made as simple as possible.
2. In each element the governing equations, usually in differential or variational (integral) form, are transformed into algebraic equation. The element equations are algebraically identical for all elements of the same type, which usually need to be derived for only one or two typical elements.
3. The resulting numbers are assembled (combined) into a much larger set of algebraic equations, which are called the system equations. In the process of element assembly, boundary conditions can be enforced automatically. Such huge systems of equations can be solved economically because the matrix of coefficients is “sparse” in essence.
4. Resulting matrix equation is then solved using suitable efficient matrix solver.



FEM seeks an approximate solution \tilde{U} , an explicit expression for U , in terms of known functions, which approximately satisfies the governing equations and boundary conditions. It obtains an approximate solution by using the classical trial-solution procedure.

Construction of a trial solution:

$$\tilde{U}(x; a) = a_0 + a_1 N_1(x) + a_2 N_2(x) + \dots + a_n N_n(x) \quad (3.1)$$

where x are the independent variables in the problems. The functions $N(x)$ are known functions called trial functions (basis). The coefficients, a , are undetermined parameters called degree of freedom (DOF).

We apply FEM to solve the new DFT formulation, as shown in Eq. (2.21), which is a typical second-order nonlinear eigenvalue problem. The purpose is to determine specific numerical values for each of the parameters a . In this FEM, we employ Galerkin weighted residual method using C^0 -linear shape function. For each parameter a_i we require that a weighted average of $R(x;a)$ over the entire domain be zero. The weighting functions of the Galerkin weighted residual method are trial functions $N(x)$ associated with each a_i .

$$\int R(x;a)N_i(x)dx \quad (3.2)$$

3.1.1 One-dimensional FEDFT Program

For the system of one nucleus with one or more electrons, Eq. (2.21) can be simplified as, by taking the spherical symmetry,

$$\varepsilon\Psi_J(r) = -\frac{1}{2}\frac{d^2}{dr^2}\Psi_J(r) - \frac{Z}{r}\Psi_J(r) + \Psi_J(r)\Pi_J(r) \quad (3.3)$$

where

$$\Pi_J = 0 \quad \text{for one-electron system } (J=1) \quad (3.4a)$$

$$\Pi_J = \frac{1}{2}H_J \quad \text{for two-electron system } (J=1) \quad (3.4b)$$

$$\Pi_J = \frac{1}{2} H_J + H_K \quad \text{for four-electron system } (J=1,2; K \neq J) \quad (3.4c)$$

$$H_J(r) = \left\langle \frac{1}{|r-r'|} \right\rangle_J = \frac{\frac{1}{r} \int_{r'=0}^r dr' |\Psi_J^{(e)}(r')|^2 r'^2 + \int_{r'=r}^{\infty} dr' |\Psi_J^{(e)}(r')|^2 r'}{\int_{r'=0}^{\infty} dr' |\Psi_J^{(e)}(r')|^2 r'^2} \quad (3.5)$$

where Ψ_J is the density function of orbital J that is limited to two electrons with spin polarization to satisfy the Pauli exclusion principle and $\Psi_J^{(e)}$ is the density function of the last evaluate. r is the radial coordinate originating from the center of the nucleus.

By applying the Galerkin weighted residual to Eq. (3.3) in a typical 1-D element,

$$\iiint R(r; \alpha) N_i(r) dv = 0, \quad i = 1, 2, \dots, n \quad (3.6)$$

where $N_i(r)$ is the shape function, $\Psi(r) \approx \tilde{U}(r; \alpha) = \sum_{j=1}^n \alpha_j N_j(r)$ and n is the number of nodes in an element. Note that the residual function, $R(r; \alpha)$, is defined as,

$$R(r; \alpha) = -\frac{1}{2} \frac{d^2}{dr^2} \tilde{U}_J(r; \alpha) - \frac{Z}{r} \tilde{U}_J(r; \alpha) + \tilde{U}_J(r; \alpha) \Pi_J - \varepsilon \tilde{U}_J(r; \alpha) \quad (3.7)$$

In the current study, linear shape function for 1-D element, $N_i(r_j) = a_i + b_i r_j = \delta_{ij}$, is used for 1-D program throughout the research, unless otherwise specified. Note that the subscripts i and j are the node numbers in a 1-D element. Substituting Eq. (3.7) into Eq. (3.6), after some algebraic arrangement [Appendix A], results in the elemental generalized eigenvalue matrix (2x2) equation that its form is rearranged to satisfy the matrix solver as

$$\{ \varepsilon [M] + [K] \} \{ \alpha \} = 0 \quad (3.8)$$

where

$$[K_{ij}] = \begin{bmatrix} -\frac{1}{5}b_i b_j \Pi_J r^5 + \frac{1}{4}[Zb_i b_j - (a_i b_j + a_j b_i)\Pi_J]r^4 + \\ \frac{1}{3}\left[Z(a_i b_j + a_j b_i) - \frac{1}{2}b_i b_j - a_i a_j \Pi_J\right]r^3 + \frac{Z}{2}a_i a_j r^2 \end{bmatrix} \quad (3.9a)$$

$$[M_{ij}] = \left[\frac{1}{5}b_i b_j r^5 + \frac{1}{4}(a_i b_j + a_j b_i)r^4 + \frac{1}{3}a_i a_j r^3 \right] \quad (3.9b)$$

Resulting system linear algebraic eigenvalue equations, obtained by assembling all elemental matrix equations as shown in Eq. (3.8), are then solved by the matrix solver by J-D method [Wang et al., 2003]. The stiffness matrix of the system equation resulting from the 1-D FEM is “marginally” diagonally dominant, from which the convergence is rather slow, which can be clearly shown in Fig. 4.17 ~ 4.18. For molecular system with more than one nucleus or with one nucleus and more than four electrons, the spherical symmetry is not held; hence, the three-dimensional FE program is required and is introduced next.

3.1.2 Three-dimensional FEDFT Program

For the system of one nucleus with one or more electrons, Eq. (2.21) can be rewritten for density function of orbital J in three-dimensional form as,

$$\varepsilon \Psi_J(\vec{r}) = -\frac{1}{2} \nabla^2 \Psi_J(\vec{r}) - \frac{Z}{\vec{r}} \Psi_J(\vec{r}) + \Psi_J(\vec{r}) \Pi_J(\vec{r}) \quad (3.10)$$

where

$$\vec{r} = (x, y, z) \quad (3.11a)$$

$$r = (x^2 + y^2 + z^2)^{1/2} \quad (3.11b)$$

$$\Pi_j(\bar{r}): \text{ the same as Eq. (3.4)} \quad (3.11c)$$

$$H_j(\bar{r}) = \langle 1/|\bar{r} - \bar{r}'| \rangle = \left\{ \int d^3\bar{r}' |\Psi_j^{(e)}(\bar{r}')|^2 / |\bar{r} - \bar{r}'| \right\} / \int d^3\bar{r}' |\Psi_j^{(e)}(\bar{r}')|^2 \quad (3.12)$$

By applying the Galerkin FEM to Eq. (3.10) in a typical 3-D element, $\Psi(\bar{r}) \approx \tilde{U}(\bar{r}; \alpha) = \sum_{j=1}^n \alpha_j N_j(\bar{r})$ and n is the number of nodes in an element. Note that $N_j(\bar{r})$ is the shape function in a typical 3-D element. Residual function, $R(\bar{r}; \alpha)$, is then defined as,

$$R(\bar{r}; \alpha) = -\frac{1}{2} \nabla^2 \tilde{U}_j(\bar{r}; \alpha) - \frac{Z}{\bar{r}} \tilde{U}_j(\bar{r}; \alpha) + \tilde{U}_j(\bar{r}; \alpha) \Pi_j - \varepsilon \tilde{U}_j(\bar{r}; \alpha) \quad (3.13)$$

In the current study, linear shape function for 3-D tetrahedral element, $N_j = \frac{a_j + b_j x + c_j y + d_j z}{6V_c}$, where V_c is the element volume, is used for 3-D program throughout the research, unless otherwise specified. Similar to the algebraic rearrangement in 1-D FEM but comparably complicated [Appendix B], the resulting elemental generalized eigenvalue matrix (4x4) equation can be written as

$$\{ \varepsilon[M] + [K] \} \{ \alpha \} = 0 \quad (3.14)$$

where

$$[M_{ij}] = \frac{V_c}{T} \quad i = j, T = 10; i \neq j, T = 20 \quad (3.15a)$$

$$[K_{ij}] = A_{ij} + B_{ij} + C_{ij} \quad (3.15b)$$

$$A_{ij} = -\frac{b_i b_j + c_i c_j + d_i d_j}{72V_c} \quad (3.15c)$$

$$B_{ij} = \frac{Z}{36V_c} \cdot \sum_{k=1}^n \frac{(a_i + b_i x_k + c_i y_k + d_i z_k)(a_j + b_j x_k + c_j y_k + d_j z_k)}{\sqrt{x_k^2 + y_k^2 + z_k^2}} w_k \quad (3.15d)$$

$$C_{ij} = -\frac{V_c}{T} \Pi_j \quad i = j, T = 10 ; i \neq j, T = 20 \quad (3.15e)$$

$$H_J(\vec{r}) = \left\langle \frac{1}{|\vec{r} - \vec{r}'|} \right\rangle_J = \frac{\iiint d^3\vec{r}' \frac{|\Psi_J^{(e)}(\vec{r}')|^2}{|\vec{r} - \vec{r}'|}}{\iiint d^3\vec{r}' |\Psi_J^{(e)}(\vec{r}')|^2} \equiv \frac{\alpha}{\beta} \quad (3.16a)$$

$$\alpha = \sum_1^{tot.element} \left[V_c \sum_{k=1}^{Gauss.points} \frac{|\Psi_J^{(e)}(\vec{r}_k)|^2}{\sqrt{(x_j - x_k)^2 + (y_j - y_k)^2 + (z_j - z_k)^2}} w_k \right] \quad (3.16b)$$

$$\beta = \sum_1^{tot.element} \left[V_c \sum_{k=1}^{Gauss.points} |\Psi_J^{(e)}(\vec{r}_k)|^2 w_k \right] \quad (3.16c)$$

Note that Gauss Quadrature [Zienkiewicz and Taylor, 2000] with weighting factor w_k at point k is used for the volume integration throughout the study, unless otherwise specified. This generalized eigenvalue formulation can be easily extended to more complicated atomic or molecular system (multiple orbits) by modifying the electron-electron interaction term, $\Pi_j(\vec{r})$, based on the Pauli exclusion principle. Resulting system equations are then assembled element by element and are solved by using J-D matrix solver similar to 1-D FE program. However, the convergence of the 3-D FE program is expected to be much faster than that in 1-D FE program due to the diagonally dominated coefficient matrix, which can be shown in Fig. 4.17 ~ 4.18.

The system equations are an eigenvalue problem with large-scale sparse matrix. Here we use the method of *random pack storage* (RPS) to just store the nonzero entries of the stiffness matrix. This method can save a lot of memories when store a large-scale sparse matrix. Resulting eigenvalue linear algebraic equations are then

solved using the Jacobi-Davidson (JD) method [Wang *et al.*, 2003], which is a subspace-type algorithm that will be introduced shortly. Overall procedures of solving the DFT eigenvalue problem can be schematically sketched in Fig. 3.1.

3.2 Jacobi-Davidson Method

The Jacobi-Davidson method [Voss and Betcke, 2002; Hwang, 2003] is based on a combination of two basic principles. The first one is to apply a Galerkin approach for the eigenproblem $Ax = \lambda x$, with respect to some given subspace spanned by an orthonormal basis $\{v_1, \dots, v_m\}$. The Galerkin condition is

$$AV_m s - \theta V_m s \perp \{v_1, \dots, v_m\} \quad V_m^* AV_m s - \theta s = 0 \quad (3.17)$$

where V_m denotes the matrix with columns v_1 to v_m . This equation has m solutions $(\theta_j^{(m)}, s_j^{(m)})$. The m pairs $(\theta_j^{(m)}, u_j^{(m)} \equiv V_m s_j^{(m)})$ are called the Ritz values and Ritz vectors of A with respect to the subspace spanned by the columns of V_m . These Ritz pairs are approximations for eigenpairs of A , and our goal is to obtain better approximations by a well-chosen expansion of the subspace.

Suppose that we have an eigenvector approximation u_j for an eigenvector x corresponding to a given eigenvalue λ . We suggested computing the orthogonal correction t for $u_j^{(m)}$.

$$A(u_j^{(m)} + t) = \lambda(u_j^{(m)} + t) \quad (3.18)$$

with $t \perp u_j^{(m)}$, $t \in U^\perp \equiv \{v \mid v^* u_j = 0\}$.

The correction equation of Jacobi-Davidson

$$(A^\perp - \theta_j I)t = -r_j \quad (3.19)$$

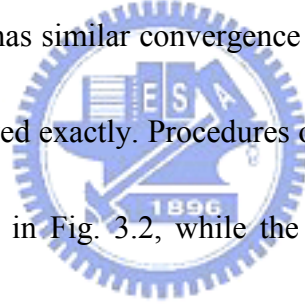
where

$$r_j = (A - \theta_j I)u_j \quad (3.20a)$$

$$A^\perp = (I - u_j u_j^*)A(I - u_j u_j^*) \quad (3.20b)$$

The next is to solve the t from Eq. (3.19) and add t into subspace to expand the search subspace, then iterate again with expansive subspace until convergence. The

Jacobi-Davidson method has similar convergence properties as inverse iteration if the correction equation is solved exactly. Procedures of solving eigenvalue problem using J-D algorithm can shown in Fig. 3.2, while the details are summarized as follows



[Wang *et al.*, 2003]:

1. Given $A(\lambda) = \lambda A_1 + A_0$
2. To choose a random vector V_i as the initial subspace
3. To compute the Galerkin condition as $M_i = V^* A_i V$.
4. To compute the Ritz pairs (θ, s) of $(\theta M_1 + M_0)s = 0$ and select the desired Ritz pair to be eigenpair with $\|s\|_2 = 1$.
5. To compute $u = Vs$, and the residual $r = A(\theta)u$.
6. If $(\|r\|_2 < \varepsilon)$, $\lambda = \theta$, $x = u$, Quit.

7. To compute correction term t and orthogonalize t against V , $v = t / \|t\|_2$
8. Expand $V = [V, v]$
9. To back to process 3 and iterate until $\|r\|_2 < \varepsilon$.

This J-D solver can efficiently deal with the large-scale sparse eigenvalue matrix equation, which is still a very challenging task even nowadays. One of the advantages in using J-D algorithm to solve the DFT eigenvalue problem is the feasibility of parallelization in the future, considering the computational demanding of the problem itself.



CHAPTER 4 RESULTS AND DISCUSSIONS

In this chapter, we first describe the elements of different cases and different computational domains and then several computational results are presented in turn.

4.1 Elements Construction

We set up two different dimensions of elements to fit the different FEDFT programs.

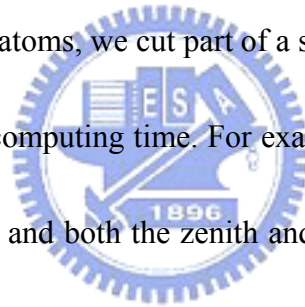
4.1.1 One-dimensional Elements

Since the simple atoms that only need to consider the s state of the angular momentum are spherical symmetry, we could simplify the computational domain of sphere to be just the radial domain. We have to set up the one-dimensional elements to match the one-dimensional FEDFT program in the radial domain. The computing radii are different for different cases (ex. the hydrogen atom is about 10 for ground state and about 20 for first excited state) but the length unit is Bohr radius, a_0 , (0.053 nm). The domain is formed by nodes and elements that two nodes compose one element in one-dimensional domain. The Fig.4.1 shows the diagram of the elements and nodes and the radial domain data of all models in this research are shown in table 4.1.

4.1.2 Three-dimensional Elements

The radial domain is only suitable for the simple atoms. When the models are many electron atoms that have to consider the other angular momentums, molecules and cluster of atoms etc. are complicated, we will have to solve the complicated problems and need the total real-space computational domain. In the three-dimensional elements, we use the tetrahedron as an element that is used for 3-D program throughout the research, unless otherwise specified and there are four nodes to compose one linear element (Fig.4.2).

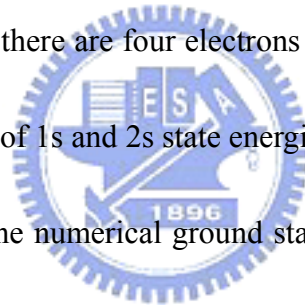
In the case of simple atoms, we cut part of a sphere to simplify the computational domain and decrease the computing time. For example the hydrogen atom, we set the radius to be 10 Bohr radii and both the zenith and azimuth angle to be 30 degrees as shown in Fig. 4.3. There are 60 nodes on the radial and 20 nodes both on the zenith and azimuth angle. The computational domain data of all models in this research are shown in table 4.2.



4.2 One-dimensional FEDFT

We take the hydrogen atom, helium-like atoms and beryllium-like atoms as models to validate the one-dimensional FEDFT program. The 1s state energies and 2s state energies of all models obtained by one-dimensional FEDFT program that are

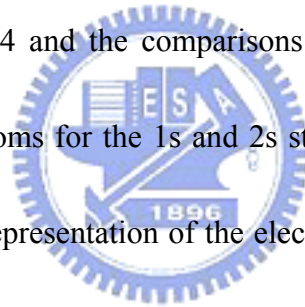
compared with the known experimental ones and numerical ones obtained by Hsu [Hsu, 2003] are shown in table 4.3 - 4.5. The numerical energies obtained by Hsu are obtained by finite difference method (FDM). The Z column shows the numbers of positive charge of the nucleus. The exp column shows the ionization energy of the electron from experiments. The $n=1$ column shows the 1s state energy of the electron from numerical results. The $n=2$ column shows the 2s state energy of the electron from numerical results. The subscripts F and H mean the numerical results by FEDFT and Hsu. The models set the different cutoff radii that all are divided by 0.001 Bohr radii as an element. Since there are four electrons in beryllium-like atoms, the ground state energy, G , is the sum of 1s and 2s state energies.



From the table 4.3, the numerical ground state energy of hydrogen atom almost conforms to the experiment. It shows that the one-dimensional FEDFT program has good performance to compute the energy of hydrogen atom. But the table 4.4 and 4.5 show that the numerical results of both FEDFT and FDM do not conform to the experiments closely. The reason should be the electron-electron interaction term that can not directly be solved by the initial equation but integrates by the last eigenvectors. The results of FEDFT are worse than FDM shown in table 4.4 and 4.5. When in one-dimensional, the matrices of both FEDFT and FDM are tri-diagonal matrices. In the current research, the stiffness matrix of the one-dimensional FEDFT is

“marginally” diagonally dominant, and it would obtain the worse solution and converge slowly.

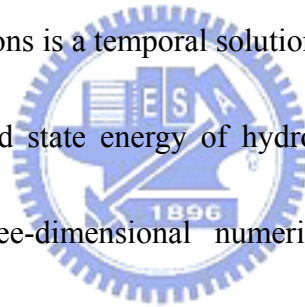
The probabilities of finding the electron in a hydrogen atom for the 1s and 2s states that are compared with exact solutions are shown in Fig. 4.4. The probabilities of finding the electron in helium-like atoms for the 1s and 2s state are shown in Fig. 4.5 ~ 4.9 and the comparisons of the probabilities of finding the electron in helium-like atoms for the 1s and 2s state are shown in Fig. 4.10 and 4.11. The probabilities of finding the electron in beryllium-like atoms for the 1s and 2s state are shown in Fig. 4.12 ~ 4.14 and the comparisons of the probabilities of finding the electron in helium-like atoms for the 1s and 2s state are shown in Fig. 4.15. Fig. 16 shows the photographic representation of the electron probability-density distribution and the numerical results conform to them.



4.3 Three-dimensional FEDFT

To solve the complicated models, we construct the three-dimensional FEDFT program. To validate the three-dimensional FEDFT program, we take the hydrogen and helium atoms to be test models. The cutoff radius is 20 Bohr radii divided by 300 nodes in radial direction, and both the zenith and azimuth angle are 30 degrees divided by 20 nodes in all angular directions for hydrogen atom model, and there are

total 165150 nodes and 796588 elements in this computational domain. The cutoff radius is 5 Bohr radii divided by 50 nodes in radial direction, and both the zenith and azimuth angle are 15 degrees divided by 15 nodes in all angular directions for helium atom model, and there are total 3668 nodes and 14629 elements in this computational domain. The numerical energies of hydrogen and helium atoms are shown in table 4.6 and 4.7. The subscripts $1d$ and $3d$ mean the numerical results obtained by one-dimensional and three-dimensional FEDFT, and H means the numerical results by Hsu. Note that the three-dimensional ground state energy of helium atom with electron-electron interactions is a temporal solution.



The numerical ground state energy of hydrogen atom almost conforms to the experiment and the three-dimensional numerical results also conform to the one-dimensional numerical ones. Although the one-dimensional and three-dimensional FEDFT both obtain the good approximation, the rate of convergence of three-dimensional FEDFT is much quicker than the one of one-dimensional FEDFT for hydrogen atom model that are shown in Fig. 4.17 ~ 4.18. Obviously, there are a lot of jumps in the convergence of one-dimensional FEDFT but it almost converges directly by three-dimensional FEDFT, mainly due to the strong diagonal dominance of the stiffness matrix in the three-dimensional FEDFT. From table 4.7, the numerical ground state energy of helium atom obtained by

three-dimensional FEDFT has a better approximation than those obtained by Hsu and one-dimensional FEDFT. It is probably due to the strong diagonal dominance of the stiffness matrix in the three-dimensional FE formulation. To compare the solutions of two kinds of FEDFT, the FEM has better performance for three-dimensional model than one-dimensional model.

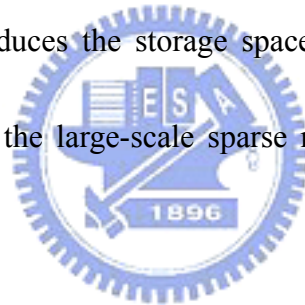
The probabilities of finding the electron in a hydrogen atom for the 1s and 2s states that are compared with exact solutions are shown in Fig. 4.19. The probability of finding the electron in a helium atom for the 1s state that is compared with one-dimensional FEDFT is shown in Fig. 4.20.



CHAPTER 5 CONCLUSIONS

In the current study, the approximations of new density-functional-theory formulation with different atoms obtained by one-dimensional and three-dimensional finite element methods that the eigenpairs of the stiffness matrices solved by Jacobi-Davidson method are presented. The major findings of the current research are summarized as follows:

1. The method of random-pack-storage that only records the value of the nonzero entries of matrices reduces the storage space of memory substantially and can avoid the problem of the large-scale sparse matrix that needs a lot of space to record all entries.
2. The matrix solver of Jacobi-Davidson method has good performance to compute the desired eigenpair of large-scale sparse matrices in an eigenproblem. It can solve rather efficiently the stiffness matrix derived from finite element method.
3. The Gauss Quadrature is a powerful numerical integration that can simplify a complicated integral and obtain a very good approximation.
4. For the same size of elements, the larger cutoff radius is, the better approximation is.
5. For hydrogen atom, the one-dimensional and three-dimensional FEDFT programs



both have good approximations of the 1s and 2s state energies.

6. The solutions of one-dimensional finite element method are worse than those of one-dimensional finite difference method for the new density-functional-theory formulation probably due to the marginally diagonal dominance of the stiffness matrix in the 1-D FE formulation.
7. Convergence rates of three-dimensional FEDFT are much faster than those of one-dimensional FEDFT, mainly due to the strong diagonal dominance of the stiffness matrix in the 3-D FE formulation.
8. For helium atom, the three-dimensional FEDFT obtains a better solution than one-dimensional FEDFT.



CHAPTER 6 FUTURE WORKS

From this study, future work is summarized as follows:

1. To confirm the three-dimensional FEDFT program that computes the helium-like and beryllium-like atoms successfully.
2. To compute the hydrogen molecule that is a two nuclei and two electrons system by the three-dimensional FEDFT program.
3. To compute the carbon atom that is a one nucleus and six electrons system and it has to consider the $2p$ orbit.
4. If the serial code performs correctly, we will parallelize it to improve the efficiency and to solve more complicated cases.



REFERENCES

1. Arias, T. A. (1999), *Multiresolution analysis of electronic structure: semicardinal and wavelet bases*, Rev. Mod. Phys., 71:267.
2. Arthur Beiser (1995), *Concepts of Modern Physics*, McGraw-Hill, New York, 216-217.
3. Bird, G.A. (1994), *Molecular Gas Dynamics and The Direct Simulation of Gas Flows*, Oxford University Press Inc., New York.
4. Burnett, David S. (1987), *Finite Element Analysis from Concepts to Applications*.....
5. Dreizler, R. M. and Gross, E. K. U. (1990), *Density Functional Theory*, Springer Verlag, Berlin.
6. Friedrich, C., Fritz Haber-Institut der Max-Planck-Gesellschaft, Berlin.
7. Harrison, N. M., *An Introduction to Density Functional Theory*.
8. Hohenberg, P. and Kohn, W. (1964), Phys Rev B, 136:864.
9. Hsu, J.Y. (2003), *Derivation of the Density Functional Theory from the Cluster Expansion*, Phys. Rev. Lett., 91:133001.
10. Hwang, T.M. (2003), *Numerical experiences of large-scale eigenvalue problems with Jacobi-Davidson method*.
11. Jan K. Labanowski (1996), *Simplified and Biased Introduction to Density Functional Approaches in Chemistry*.
12. Kimball, G. E., and Shortley, G. H. (1934), Phys. Rev., 45:815.
13. Kohn, W and Sham, L.J. (1965), Phys Rev A, 140:1133.
14. Kohn, W. (1999), *Electronic structure of matter—wave functions and density functionals*, Rev. Mod. Phys., 71:1253.
15. Markus Oppel (2002), *DFT – Density functional theory*.
16. Michael P. Marder. (2000), *Condensed matter physics*.
17. Ohno, K., Esfarjani, K., and Kawazoe, Y. (1999), *computational materials science (from ab-initio to Monte Carlo methods)*. Springer-Verlag, Berlin.
18. Olson, G.B. (1997), *Science*; 277:1237.
19. Pauling, L., and Wilson, E. B. (1935), *Introduction to Quantum Mechanics*, Dover, New York, p. 202.
20. Perdew, J. P. and Wang, Y. (1986), *Phys. Rev. B* 33, 8800; *Ibid. E* 34, 7406.
21. Schöne, Wolf-Dieter, *Density-functional theory and the Kohn-Sham equations*.
22. Schrödinger, E. (1926), *Am. Physik* 79, 361.
23. Seminario, J.M., and Politzer, P. ed. (1995), *Modern Density Functional Theory: A Tool for Chemistry*, Elsevier.
24. Stephen Jenkins (1997), *The Many Body Problem and Density Functional*

Theory,

<http://newton.ex.ac.uk/research/semiconductors/theory/people/jenkins/mbody/mbody3.html> .

25. Strang, G., and Fix, G. J. (1973), *An Analysis of the Finite Element Method*, Prentice-Hall, Englewood Cliffs.
26. Thomas L. Beck (2000), *Real-space mesh techniques in density functional theory*, Reviews of Modern Physics.
27. Voss, H. and Betcke, T. (2002), *A Jacobi-Davidson-type projection method for nonlinear eigenvalue problems*, preprint submitted to Elsevier Science.
28. Wadley, H.N.G., Zhou, X., Johnson R.A., and Neurock, M. (2001), *Mechanisms, models and methods of vapor deposition*, Progress in Materials Science, 46:329-377.
29. Wang, W., Hwang, T.-M. Lin, W.-W. and Liu, J.-L. (2003), *Numerical methods for semiconductor heterostructures with band nonparabolicity*, J. Comp. Phys., 190:141-158.
30. Wu, J.-S. and Hsu, K.-H. (2004), *Progress Towards Parallel Particle Modeling of DC-Magnetron Sputtering Plasma*, 24th International Symposium on Rarefied Gas Dynamics, July 10-16, 2004, Bari, Italy.
31. Wu, J.-S., Tseng, K.-C. and Wu, F.-Y. (2004), *Parallel Three-Dimensional DSMC Method Using Mesh Refinement and Variable Time-Step Scheme*, Computer Physics Communications (accept).
32. Zienkiewicz, O.C. and Taylor, R.L. (2000), *The Finite Element Method: The Basis*, Butterworth-Heinemann, 219-223.

APPENDIX A

One-Dimensional FEDFT

In this appendix, we provide the detail of the one-dimensional finite element form of the new DFT formulation from the governing equation to the system equation. We will use the Galerkin weighted residual method [Burnett, 1987] throughout the research, unless otherwise specified.

The general governing equation is written as [Hsu, 2003]

$$\varepsilon\Psi_0(\bar{r}) = -\frac{1}{2}\nabla^2\Psi_0(\bar{r}) - \sum_I \frac{Z_I}{|\bar{r} - \bar{R}_I|} \Psi_0(\bar{r}) + \frac{1}{2}(N-1)\Psi_0(\bar{r}) \left\langle \frac{1}{|\bar{r} - \bar{r}'|} \right\rangle \quad (\text{A.1a})$$

$$\left\langle \frac{1}{|\bar{r} - \bar{r}'|} \right\rangle = \frac{\int d\tau' \frac{|\Psi_0(\bar{r}')|^2}{|\bar{r} - \bar{r}'|}}{\int d\tau' |\Psi_0(\bar{r}')|^2} \quad (\text{A.1b})$$

where Ψ_0 is the density function, r and R is the coordinate from the zero point of the computing space, Z is the number of positive charge of the nucleus, the subscript I means the kind of nucleus and N is the number of electrons.

For the system of one nucleus that is the simple atom like hydrogen or helium atom with one or more electrons, Eq. (A.1) can be simplified as, by taking the spherical symmetry,

$$\varepsilon\Psi_J(r) = -\frac{1}{2} \frac{d^2}{dr^2} \Psi_J(r) - \frac{Z}{r} \Psi_J(r) + \Psi_J(r) \Pi_J(r) \quad (\text{A.2})$$

where

$$\Pi_J = 0 \quad \text{for one-electron system } (J=1) \quad (\text{A.3a})$$

$$\Pi_J = \frac{1}{2} H_J \quad \text{for two-electron system } (J=1) \quad (\text{A.3b})$$

$$\Pi_J = \frac{1}{2} H_J + H_K \quad \text{for four-electron system } (J=1,2; K \neq J) \quad (\text{A.3c})$$

$$H_J(r) = \left\langle \frac{1}{|r-r'|} \right\rangle_J = \left\{ \int dr' \frac{|\Psi_J(r')|^2}{|r-r'|} \right\} / \int dr' |\Psi_J(r')|^2 \quad (\text{A.4})$$

where Ψ_J is the density function of orbital J that is limited to two electrons with spin polarization to satisfy the Pauli exclusion principle and r is the radial coordinate originating from the center of the nucleus.

We construct a trial solution to approximate the density function $\Psi(r) \approx \tilde{U}(r; \alpha)$.

The typical 1-D element trial solution can always be written in the general form,

$$\tilde{U}(r; \alpha) = \sum_{j=1}^n \alpha_j N_j(r) \quad (\text{A.5})$$

The coefficients $\alpha_1, \alpha_2, \dots, \alpha_n$ are undetermined parameters, frequently called *degrees of freedom* (DOF). We would say that $\tilde{U}(r; \alpha)$ in Eq. (A.5) has n DOF. In the following theoretical development, the first three steps are short, formal operations using only the general form Eq. (A.5). It is not until step 4 that we decide on the value of n and the specific form of each of the shape functions $N_j(r)$.

Step 1 : Write the Galerkin residual equations for a typical element.

The residual for Eq. (A.2) is

$$R(r; \alpha) = -\frac{1}{2} \frac{d^2}{dr^2} \tilde{U}_J(r; \alpha) - \frac{Z}{r} \tilde{U}_J(r; \alpha) + \tilde{U}_J(r; \alpha) \Pi_J - \varepsilon \tilde{U}_J(r; \alpha) \quad (\text{A.6})$$

We need one residual equation for each DOF in Eq. (A.5):

$$\iiint R(r; \alpha) N_i(r) dv = 0 \quad i = 1, 2, \dots, n \quad (\text{A.7})$$

where the integration integrate over one element and n is the number of nodes in an

element. Substituting Eq. (A.5) into Eq. (A.7) yields

$$\int \left[-\frac{1}{2} \frac{d^2}{dr^2} \tilde{U}_J(r; \alpha) - \frac{Z}{r} \tilde{U}_J(r; \alpha) + \tilde{U}_J(r; \alpha) \Pi_J - \varepsilon \tilde{U}_J(r; \alpha) \right] N_i(r) (4\pi r^2) dr = 0 \quad (\text{A.8})$$

$i = 1, 2, \dots, n$

Step 2 : Integrate by parts.

The second derivative term is integrated by parts once:

$$\begin{aligned} & \frac{1}{2} \int r^2 \frac{dN_i(r)}{dr} \frac{d\tilde{U}_J(r; \alpha)}{dr} dr - Z \int r N_i(r) \tilde{U}_J(r; \alpha) dr + \int r^2 N_i(r) \tilde{U}_J(r; \alpha) \Pi_J dr \\ & - \varepsilon \int r^2 N_i(r) \tilde{U}_J(r; \alpha) = - \left[\left(-\frac{r^2}{2} \frac{d}{dr} \tilde{U}_J(r; \alpha) \right) N_i(r) \right]_{r_1}^{r_n} \quad i = 1, 2, \dots, n \end{aligned} \quad (\text{A.9})$$

where r_1, r_n are the two boundary nodes of the element.

The boundary term contains, as usual, the flux,

$$- \left[\left(-\frac{r^2}{2} \frac{d}{dr} \tilde{U}_J(r; \alpha) \right) N_i(r) \right]_{r_1}^{r_n} = [\tilde{\tau}(r; \alpha) N_i]_{r_1}^{r_n} \quad (\text{A.10})$$

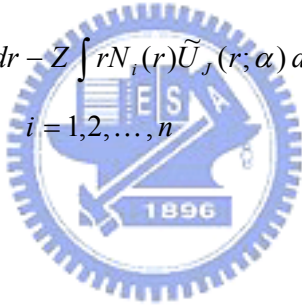
As is characteristic of eigenproblems, there cannot be any loads. Thus the interior

load is zero, and the boundary conditions must be zero. For the eigenproblems, the

boundary term contains the flux must vanish from the system equations. The

boundary term occurs in two different ways in the system equations: at each node on

the boundary of the domain, and as the difference of two such expressions at each node on inter-element boundaries. In the first case, the boundary conditions require that the term vanish at the domain boundary nodes. In the second case, a nonzero difference in flux at an inter-element boundary represents an applied concentrated load; however, the eigenproblems does not permit applied loads. Since the boundary term must vanish from the system equations, we will ignore it right at the outset by eliminating it from the element equations. Therefore Eq. (A.9) may be written as follows:

$$\frac{1}{2} \int r^2 \frac{dN_i(r)}{dr} \frac{d\tilde{U}_j(r; \alpha)}{dr} dr - Z \int r N_i(r) \tilde{U}_j(r; \alpha) dr + \int r^2 N_i(r) \tilde{U}_j(r; \alpha) \Pi_j dr - \varepsilon \int r^2 N_i(r) \tilde{U}_j(r; \alpha) = 0 \quad i = 1, 2, \dots, n \quad (\text{A.11})$$


Step 3 : Substitute the general form of the element trial solution into integrals in residual equations. Inserting Eq. (A.5) into Eq. (A.11) yields

$$\frac{1}{2} \sum_{j=1}^n \left[\int r^2 \frac{dN_i(r)}{dr} \frac{dN_j(r)}{dr} dr \right] \alpha_j - Z \sum_{j=1}^n \left[\int r N_i(r) N_j(r) dr \right] \alpha_j + \sum_{j=1}^n \left[\int r^2 N_i(r) N_j(r) \Pi_j dr \right] \alpha_j - \varepsilon \sum_{j=1}^n \left[\int r^2 N_i(r) N_j(r) dr \right] \alpha_j = 0 \quad i = 1, 2, \dots, n \quad (\text{A.12})$$

These are the element equations for a typical element.

Eq. (A.12) may be written in conventional matrix form that is rearranged to satisfy the matrix solver as:

$$\{\varepsilon[M] + [K]\}\{\alpha\} = 0 \quad (\text{A.13})$$

where

$$K_{ij} = -\frac{1}{2} \int r^2 \frac{dN_i(r)}{dr} \frac{dN_j(r)}{dr} dr + Z \int r N_i(r) N_j(r) dr - \int r^2 N_i(r) N_j(r) \Pi_J dr \quad (\text{A.14a})$$

$$M_{ij} = \int r^2 N_i N_j dr \quad (\text{A.14b})$$

Step 4 : Develop specific expressions for the shape functions $N_j(r)$

We use the two-node linear element to be the 1-D typical element (Fig. 4.1). For convenience, we repeat those results here:

$$\tilde{U}(r; \alpha) = \sum_{j=1}^2 \alpha_j N_j(r) \quad (\text{A.15})$$

where the shape functions possess the requisite interpolation property,

$$N_j(r_k) = a_j + b_j r_k = \delta_{jk} \quad (\text{A.16a})$$

$$j=1 \Rightarrow a_1 = \frac{r_2}{r_2 - r_1} \quad b_1 = -\frac{r}{r_2 - r_1} \quad (\text{A.16b})$$

$$j=2 \Rightarrow a_2 = -\frac{r_1}{r_2 - r_1} \quad b_2 = \frac{r}{r_2 - r_1} \quad (\text{A.16c})$$

This element is frequently referred to as a C^0 -linear element, in obvious reference to the continuity and completeness properties it process.

Step 5 : Substitute the shape functions into the element equations, and transform the integrals into a form appropriate for numerical evaluation.

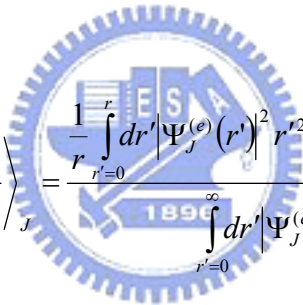
Substitute Eq. (A.16) into Eq. (A.14) :

$$\begin{aligned}
K_{ij} &= \int -\frac{1}{2} b_i b_j r^2 + Z(a_i + b_i r)(a_j + b_j r)r - \Pi_J(a_i + b_i r)(a_j + b_j r)r^2 dr \\
&= -\frac{1}{5} b_i b_j \Pi_J r^5 + \frac{1}{4} [Z b_i b_j - (a_i b_j + a_j b_i) \Pi_J] r^4 \\
&\quad + \frac{1}{3} \left[Z(a_i b_j + a_j b_i) - \frac{1}{2} b_i b_j - a_i a_j \Pi_J \right] r^3 + \frac{Z}{2} a_i a_j r^2
\end{aligned} \tag{A.17a}$$

$$M_{ij} = \int (a_i + b_i r)(a_j + b_j r)r^2 dr = \frac{1}{5} b_i b_j r^5 + \frac{1}{4} (a_i b_j + a_j b_i) r^4 + \frac{1}{3} a_i a_j r^3 \tag{A.17b}$$

Step 6 : Derive expression for the Π_J .

The nonlinear term, Π_J , in the Eq. (A.2) describes as Eq. (A.3). The $1/|r-r'|$ of the integration, H_J , may expand the solutions in terms of the Legendre polynomials yields



$$H_J(r) = \left\langle \frac{1}{|r-r'|} \right\rangle_J = \frac{\frac{1}{r} \int_{r'=0}^r dr' |\Psi_J^{(e)}(r')|^2 r'^2 + \int_{r'=r}^{\infty} dr' |\Psi_J^{(e)}(r')|^2 r'}{\int_{r'=0}^{\infty} dr' |\Psi_J^{(e)}(r')|^2 r'^2} \tag{A.18}$$

$\Psi_J^{(e)}$ is the density function of the last evaluate.

This completes the six steps for deriving the element equations. After performing the addition operations, all elemental matrix equations are assembled to be system equations that are then solved by J-D matrix solver.

APPENDIX B

Three-Dimensional FEDFT

In this appendix, we provide the detail of the three-dimensional finite element form of the new DFT formulation from the governing equation to the system equation. We will use the Galerkin weighted residual method [Burnett, 1987] throughout the research, unless otherwise specified.

The general governing equation is written as [Hsu, 2003]

$$\varepsilon\Psi_0(\vec{r}) = -\frac{1}{2}\nabla^2\Psi_0(\vec{r}) - \sum_I \frac{Z_I}{|\vec{r} - \vec{R}_I|} \Psi_0(\vec{r}) + \frac{1}{2}(N-1)\Psi_0(\vec{r}) \left\langle \frac{1}{|\vec{r} - \vec{r}'|} \right\rangle \quad (\text{B.1a})$$

$$\left\langle \frac{1}{|\vec{r} - \vec{r}'|} \right\rangle = \frac{\int d\tau' \frac{|\Psi_0(\vec{r}')|^2}{|\vec{r} - \vec{r}'|}}{\int d\tau' |\Psi_0(\vec{r}')|^2} \quad (\text{B.1b})$$

where Ψ_0 is the density function, r and R is the coordinate from the zero point of the computing space, Z is the number of positive charge of the nucleus, the subscript I means the kind of nucleus and N is the number of electrons.

For the system of one nucleus with one or more electrons, Eq. (B1) can be rewritten for density function of orbital J in three-dimensional form as,

$$\varepsilon\Psi_J(\vec{r}) = -\frac{1}{2}\nabla^2\Psi_J(\vec{r}) - \frac{Z}{r} \Psi_J(\vec{r}) + \Psi_J(\vec{r})\Pi_J(\vec{r}) \quad (\text{B.2})$$

where

$$\vec{r} = (x, y, z) \quad (\text{B.3a})$$

$$r = (x^2 + y^2 + z^2)^{1/2} \quad (\text{B.3b})$$

$$\Pi_J = 0 \quad \text{for one-electron system } (J=1) \quad (\text{B.3c})$$

$$\Pi_J = \frac{1}{2} H_J \quad \text{for two-electron system } (J=1) \quad (\text{B.3d})$$

$$\Pi_J = \frac{1}{2} H_J + H_K \quad \text{for four-electron system } (J=1,2; K \neq J) \quad (\text{B.3e})$$

$$H_J(\bar{r}) = \langle 1/|\bar{r} - \bar{r}'| \rangle = \left\{ \int d^3\bar{r}' |\Psi_J^{(e)}(\bar{r}')|^2 / |\bar{r} - \bar{r}'| \right\} / \int d^3\bar{r}' |\Psi_J^{(e)}(\bar{r}')|^2 \quad (\text{B.4})$$

where Ψ_J is the density function of orbital J that is limited to two electrons with spin polarization to satisfy the Pauli exclusion principle and r is the radial coordinate originating from the center of the nucleus.

We construct a trial solution to approximate the density function $\Psi(r) \approx \tilde{U}(r; \alpha)$.

The typical 3-D element trial solution can always be written in the general form,

$$\tilde{U}(\bar{r}; \alpha) = \sum_{j=1}^n \alpha_j N_j(\bar{r}) \quad (\text{B.5})$$

In the current study, linear shape function for 3-D tetrahedral element is used for 3-D program throughout the research, unless otherwise specified.

Step 1 : Write the Galerkin residual equations for a typical element.

The residual for Eq. (B.2) is

$$R(\bar{r}; \alpha) = -\frac{1}{2} \nabla^2 \tilde{U}_J(\bar{r}; \alpha) - \frac{Z}{\bar{r}} \tilde{U}_J(\bar{r}; \alpha) + \tilde{U}_J(\bar{r}; \alpha) \Pi_J - \varepsilon \tilde{U}_J(\bar{r}; \alpha) \quad (\text{B.6})$$

We need one residual equation for each DOF in Eq. (B.5):

$$\iiint R(\bar{r}; \alpha) N_i(\bar{r}) dv = 0 \quad i = 1, 2, \dots, n \quad (\text{B.7})$$

where the integration integrate over one element and n is the number of nodes in an

element. Substituting Eq. (B.5) into Eq. (B.7) yields

$$\iiint \left[-\frac{1}{2} \nabla^2 \tilde{U}_J(\bar{r}; \alpha) - \frac{Z}{\bar{r}} \tilde{U}_J(\bar{r}; \alpha) + \tilde{U}_J(\bar{r}; \alpha) \Pi_J - \varepsilon \tilde{U}_J(\bar{r}; \alpha) \right] N_i(\bar{r}) d\bar{r}^3 = 0 \quad (\text{B.8})$$

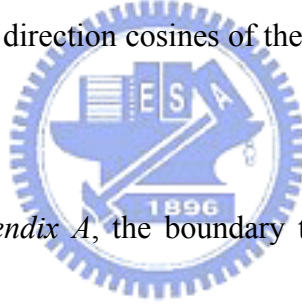
$i = 1, 2, \dots, n$

Step 2 : Integrate by parts.

The second derivative term is integrated by parts once:

$$\begin{aligned} & \frac{1}{2} \iiint \left[\frac{\partial N_i(\bar{r})}{\partial x} \frac{\partial \tilde{U}_J(\bar{r}; \alpha)}{\partial x} + \frac{\partial N_i(\bar{r})}{\partial y} \frac{\partial \tilde{U}_J(\bar{r}; \alpha)}{\partial y} + \frac{\partial N_i(\bar{r})}{\partial z} \frac{\partial \tilde{U}_J(\bar{r}; \alpha)}{\partial z} \right] d\bar{r}^3 - Z \iiint \frac{N_i(\bar{r}) \tilde{U}_J(\bar{r}; \alpha)}{\bar{r}} d\bar{r}^3 \\ & + \iiint \Pi_J N_i(\bar{r}) \tilde{U}_J(\bar{r}; \alpha) d\bar{r}^3 - \varepsilon \iiint N_i(\bar{r}) \tilde{U}_J(\bar{r}; \alpha) d\bar{r}^3 \\ & = \frac{1}{2} \iint \left[\left(\frac{\partial \tilde{U}}{\partial x} \right) N_i n_x dydz + \left(\frac{\partial \tilde{U}}{\partial y} \right) N_i n_y dzdx + \left(\frac{\partial \tilde{U}}{\partial z} \right) N_i n_z dxdy \right] \end{aligned} \quad (\text{B.9})$$

where n_x , n_y and n_z are the direction cosines of the outward unit normal to the element boundary.



As the same in *Appendix A*, the boundary term contains the flux must vanish from the system equations for the eigenproblems. We will ignore it right at the outset by eliminating it from the element equations. Therefore Eq. (B.9) may be written as follows:

$$\begin{aligned} & \frac{1}{2} \iiint \left[\frac{\partial N_i(\bar{r})}{\partial x} \frac{\partial \tilde{U}_J(\bar{r}; \alpha)}{\partial x} + \frac{\partial N_i(\bar{r})}{\partial y} \frac{\partial \tilde{U}_J(\bar{r}; \alpha)}{\partial y} + \frac{\partial N_i(\bar{r})}{\partial z} \frac{\partial \tilde{U}_J(\bar{r}; \alpha)}{\partial z} \right] d\bar{r}^3 - Z \iiint \frac{N_i(\bar{r}) \tilde{U}_J(\bar{r}; \alpha)}{\bar{r}} d\bar{r}^3 \\ & + \iiint \Pi_J N_i(\bar{r}) \tilde{U}_J(\bar{r}; \alpha) d\bar{r}^3 - \varepsilon \iiint N_i(\bar{r}) \tilde{U}_J(\bar{r}; \alpha) d\bar{r}^3 = 0 \end{aligned} \quad (\text{B.10})$$

Step 3 : Substitute the general form of the element trial solution into integrals in residual equations. Inserting Eq. (B.5) into Eq. (B.10) yields

$$\begin{aligned}
& \frac{1}{2} \sum_{j=1}^n \left[\iiint \frac{\partial N_i(\bar{r})}{\partial x} \frac{\partial N_j(\bar{r})}{\partial x} + \frac{\partial N_i(\bar{r})}{\partial y} \frac{\partial N_j(\bar{r})}{\partial y} + \frac{\partial N_i(\bar{r})}{\partial z} \frac{\partial N_j(\bar{r})}{\partial z} d\bar{r}^3 \right] \alpha_j \\
& - Z \sum_{j=1}^n \left[\iiint \frac{N_i(\bar{r}) N_j(\bar{r})}{\bar{r}} d\bar{r}^3 \right] \alpha_j + \sum_{j=1}^n \left[\iiint \Pi_j N_i(\bar{r}) N_j(\bar{r}) d\bar{r}^3 \right] \alpha_j \quad (\text{B.11}) \\
& - \varepsilon \sum_{j=1}^n \left[\iiint N_i(\bar{r}) N_j(\bar{r}) d\bar{r}^3 \right] \alpha_j = 0 \quad i = 1, 2, \dots, n
\end{aligned}$$

These are the element equations for a typical element.

Eq. (B.11) may be written in conventional matrix form that is rearranged to satisfy the matrix solver as:

$$\{ \varepsilon [M] + [K] \} \{ \alpha \} = 0 \quad (\text{B.12})$$

where

$$\begin{aligned}
K_{ij} = & -\frac{1}{2} \iiint \frac{\partial N_i(\bar{r})}{\partial x} \frac{\partial N_j(\bar{r})}{\partial x} + \frac{\partial N_i(\bar{r})}{\partial y} \frac{\partial N_j(\bar{r})}{\partial y} + \frac{\partial N_i(\bar{r})}{\partial z} \frac{\partial N_j(\bar{r})}{\partial z} d\bar{r}^3 \\
& + Z \iiint \frac{N_i(\bar{r}) N_j(\bar{r})}{\bar{r}} d\bar{r}^3 - \iiint \Pi_j N_i(\bar{r}) N_j(\bar{r}) d\bar{r}^3 \quad (\text{B.13a})
\end{aligned}$$

$$M_{ij} = \iiint N_i(\bar{r}) N_j(\bar{r}) d\bar{r}^3 \quad (\text{B.13b})$$

Step 4 : Develop specific expressions for the shape functions $N_j(r)$

We use the linear tetrahedral element to be the 3-D typical element (Fig. 4.2).

The typical 3-D element trial solution can be written

$$\tilde{U}(\bar{r}; \alpha) = \sum_{j=1}^4 \alpha_j N_j(x, y, z) \quad (\text{B.14})$$

The special coordinates are introduced defined by (Fig. B.1) :

$$x = L_1 x_1 + L_2 x_2 + L_3 x_3 + L_4 x_4 \quad (\text{B.15a})$$

$$y = L_1 y_1 + L_2 y_2 + L_3 y_3 + L_4 y_4 \quad (\text{B.15b})$$

$$z = L_1 z_1 + L_2 z_2 + L_3 z_3 + L_4 z_4 \quad (\text{B.15c})$$

$$1 = L_1 + L_2 + L_3 + L_4 \quad (\text{B.15d})$$

Solving Eq. (B.15) gives $L_j = \frac{a_j + b_j x + c_j y + d_j z}{6V_c}$ etc. The linear shape functions for

the linear element are simply

$$N_1 = L_1 \quad N_2 = L_2 \quad \text{etc.} \quad (\text{B.16})$$

where V_c represents the volume of the tetrahedron.

$$V_c = \frac{1}{6} \begin{vmatrix} 1 & x_1 & y_1 & z_1 \\ 1 & x_2 & y_2 & z_2 \\ 1 & x_3 & y_3 & z_3 \\ 1 & x_4 & y_4 & z_4 \end{vmatrix} \quad (\text{B.17a})$$

$$a_j = \begin{vmatrix} x_k & y_k & z_k \\ x_l & y_l & z_l \\ x_m & y_m & z_m \end{vmatrix} \quad (\text{B.17b})$$

$$b_j = - \begin{vmatrix} 1 & y_k & z_k \\ 1 & y_l & z_l \\ 1 & y_m & z_m \end{vmatrix} \quad (\text{B.17c})$$

$$c_j = - \begin{vmatrix} x_k & 1 & z_k \\ x_l & 1 & z_l \\ x_m & 1 & z_m \end{vmatrix} \quad (\text{B.17d})$$

$$d_j = - \begin{vmatrix} x_k & y_k & 1 \\ x_l & y_l & 1 \\ x_m & y_m & 1 \end{vmatrix} \quad (\text{B.17e})$$

Step 5 : Substitute the shape functions into the element equations, and transform

the integrals into a form appropriate for numerical evaluation.

Substitute Eq. (B.16) into Eq. (B.13) :

$$\begin{aligned} M_{ij} &= \iiint N_i(\bar{r})N_j(\bar{r}) d\bar{r}^3 = \frac{V_c}{10} \quad (\text{if } i = j) \\ &= \frac{V_c}{20} \quad (\text{if } i \neq j) \end{aligned} \quad (\text{B.18a})$$

$$K = A + B + C \quad (\text{B.18b})$$

$$A = -\frac{1}{2} \iiint \frac{\partial N_i(\bar{r})}{\partial x} \frac{\partial N_j(\bar{r})}{\partial x} + \frac{\partial N_i(\bar{r})}{\partial y} \frac{\partial N_j(\bar{r})}{\partial y} + \frac{\partial N_i(\bar{r})}{\partial z} \frac{\partial N_j(\bar{r})}{\partial z} d\bar{r}^3 = -\frac{b_i b_j + c_i c_j + d_i d_j}{72 V_c} \quad (\text{B.18c})$$

by Gauss Quadrature (GQ):

$$\begin{aligned} B &= Z \iiint \frac{N_i(\bar{r})N_j(\bar{r})}{\bar{r}} d\bar{r}^3 \\ &= \frac{Z}{36V_c} \cdot \sum_{k=1}^G \frac{(a_i + b_i x_k + c_i y_k + d_i z_k)(a_j + b_j x_k + c_j y_k + d_j z_k)}{\sqrt{x_k^2 + y_k^2 + z_k^2}} w_k \end{aligned} \quad (\text{B.18d})$$

where G is the total numbers of the Gauss point, w_k is the weighting factor and the subscript k means that the related values on the Gauss point (Table B.1) [Zienkiewicz and Taylor, 2000]. We will use the quadratic of GQ throughout the research, unless otherwise specified.

$$\begin{aligned} C_{ij} &= -\iiint \Pi_j N_i(\bar{r})N_j(\bar{r}) d\bar{r}^3 = -\frac{V_c}{10} \Pi_j \quad (\text{if } i = j) \\ &= -\frac{V_c}{20} \Pi_j \quad (\text{if } i \neq j) \end{aligned} \quad (\text{B.18e})$$

Step 6 : Derive expression for the Π_j .

The nonlinear term, Π_j , in the Eq. (B.2) describes as Eq. (B.3). The integration,

H_J , integrate by Gauss Quadrature.

$$H_J(\vec{r}) = \left\langle \frac{1}{|\vec{r} - \vec{r}'|} \right\rangle_J = \frac{\iiint d^3\vec{r}' \frac{|\Psi_J^{(e)}(\vec{r}')|^2}{|\vec{r} - \vec{r}'|}}{\iiint d^3\vec{r}' |\Psi_J^{(e)}(\vec{r}')|^2} \equiv \frac{\alpha}{\beta} \quad (\text{B.19a})$$

$$\alpha = \sum_1^{\text{tot. element}} \left[V_c \sum_{k=1}^G \frac{|\Psi_J^{(e)}(\vec{r}_k)|^2}{\sqrt{(x_j - x_k)^2 + (y_j - y_k)^2 + (z_j - z_k)^2}} w_k \right] \quad (\text{B.19b})$$

$$\beta = \sum_1^{\text{tot. element}} \left[V_c \sum_{k=1}^G |\Psi_J^{(e)}(\vec{r}_k)|^2 w_k \right] \quad (\text{B.19c})$$

$\Psi_J^{(e)}$ is the density function of the last evaluate.

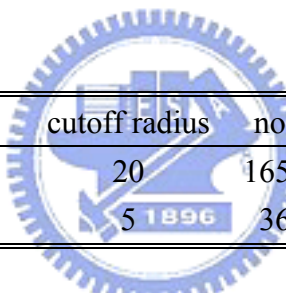
This completes the six steps for deriving the element equations. After performing the addition operations, all elemental matrix equations are assembled to be system equations that are then solved by J-D matrix solver.



Table 4.1 The radial domain data of all models for one-dimensional FEDFT in this research. Cutoff radius is in units of Bohr radius.

Atom	cutoff radius	nodes	elements
H	20	20001	20000
He	10	10001	10000
Li ⁺	6	6001	6000
Be ⁺²	5	5001	5000
B ⁺³	4	4001	4000
C ⁺⁴	3	3001	3000
Be	6	6001	6000
B ⁺	5	5001	5000
C ⁺²	4	4001	4000

Table 4.2 The computational domain data of all models for three-dimensional FEDFT in this research. Cutoff radius is in units of Bohr radius.



Atom	cutoff radius	nodes	elements
H	20	165150	796588
He	5	3668	14629

Table 4.3 Hydrogen atom. The energies of the electron obtained by one-dimensional FEDFT program compared with experiment. Energy is in units of eV.

Atom	Z	exp	$n=1_F$	$n=2_F$
H	1	13.6	13.60002372	3.400007348

Table 4.4 Helium-like atoms. The energies of the electron obtained by one-dimensional FEDFT program compared with experimental ones and numerical ones obtained by Hsu. Energy is in units of eV.

Atom	Z	exp	n=1 _H	n=2 _H	n=1 _F	n=2 _F
He	2	79	78	19	77.10271484	19.46709836
Li ⁺	3	198	196	50	196.0677136	49.34028086
Be ⁺²	4	371	370	93	369.4731368	92.84837742
B ⁺³	5	600	598	150	597.2802483	149.9571332
C ⁺⁴	6	882	880	220	879.4880575	220.6660783

Table 4.5 Beryllium-like atoms. The energies of the electron obtained by one-dimensional FEDFT program compared with experimental ones and numerical ones obtained by Hsu. Energy is in units of eV.

Atom	Z	exp	G_H	G_F
Be	4	399	390	387.5745747
B ⁺	5	663	662	649.4520744
C ⁺²	6	991	989	979.4498507

Table 4.6 Hydrogen atom. The energies of the electron obtained by three-dimensional FEDFT program compared with experimental ones and numerical ones obtained by one-dimensional FEDFT. Energy is in units of eV.

Atom	Z	exp	n=1 _{1d}	n=2 _{1d}	n=1 _{3d}	n=2 _{3d}
H	1	13.6	13.60002372	3.400007348	13.6006394	3.399937991

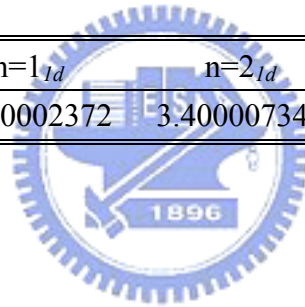


Table 4.7 Helium atom. The energies of the electron obtained by three-dimensional FEDFT program compared with experimental ones and numerical ones obtained by Hsu and one-dimensional FEDFT. Energy is in units of eV.

Atom	Z	exp	$n=1_H$	$n=1_{1d}$	$n=1_{3d}$
He	2	79	78	77.10271	78.34722

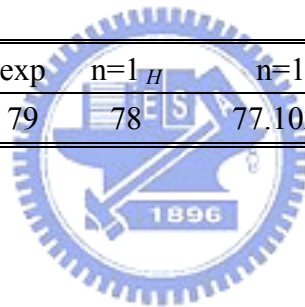
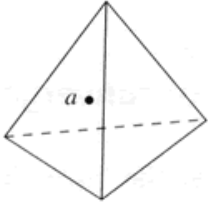
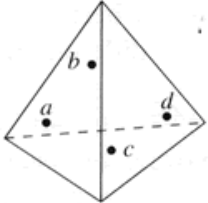
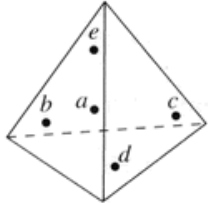


Table B.1 Numerical integration formula of Gauss Quadrature for tetrahedral element [Zienkiewicz and Taylor, 2000].

No.	Order	Figure	Error	Points	Tetrahedral coordinates	Weights
1	Linear		$R = O(h^2)$	a	$\frac{1}{4}, \frac{1}{4}, \frac{1}{4}, \frac{1}{4}$	1
2	Quadratic		$R = O(h^3)$	a b c d	$\left. \begin{array}{l} \alpha, \beta, \beta, \beta \\ \beta, \alpha, \beta, \beta \\ \beta, \beta, \alpha, \beta \\ \beta, \beta, \beta, \alpha \end{array} \right\}$ $\alpha = 0.58541020$ $\beta = 0.13819660$	$\frac{1}{4}$
3	Cubic		$R = O(h^4)$	a b c d e	$\left. \begin{array}{l} \frac{1}{4}, \frac{1}{4}, \frac{1}{4}, \frac{1}{4} \\ \frac{1}{2}, \frac{1}{6}, \frac{1}{6}, \frac{1}{6} \\ \frac{1}{6}, \frac{1}{2}, \frac{1}{6}, \frac{1}{6} \\ \frac{1}{6}, \frac{1}{6}, \frac{1}{2}, \frac{1}{6} \\ \frac{1}{6}, \frac{1}{6}, \frac{1}{6}, \frac{1}{2} \end{array} \right\}$	$-\frac{4}{5}$ $\frac{9}{20}$

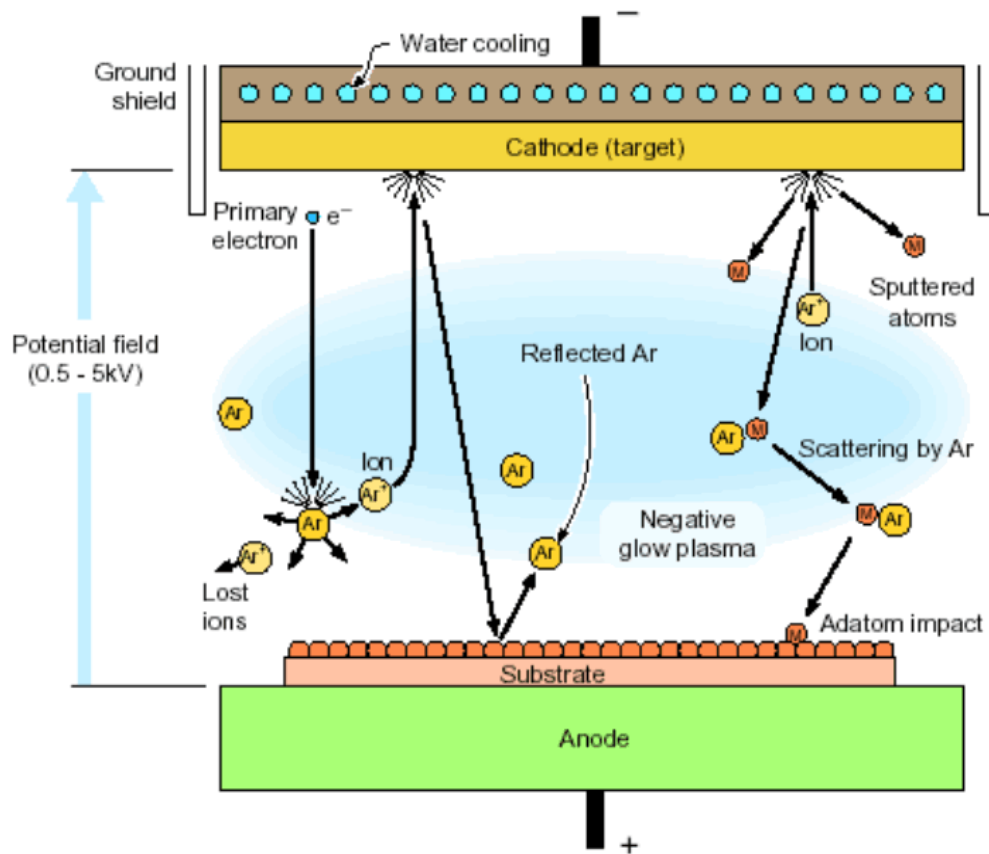


Fig. 1.1 Sketch of the multiscale and physical processes in a DC-magnetron sputtering chamber.

MULTISCALE MODELLING TOOLS FOR VAPOR DEPOSITION

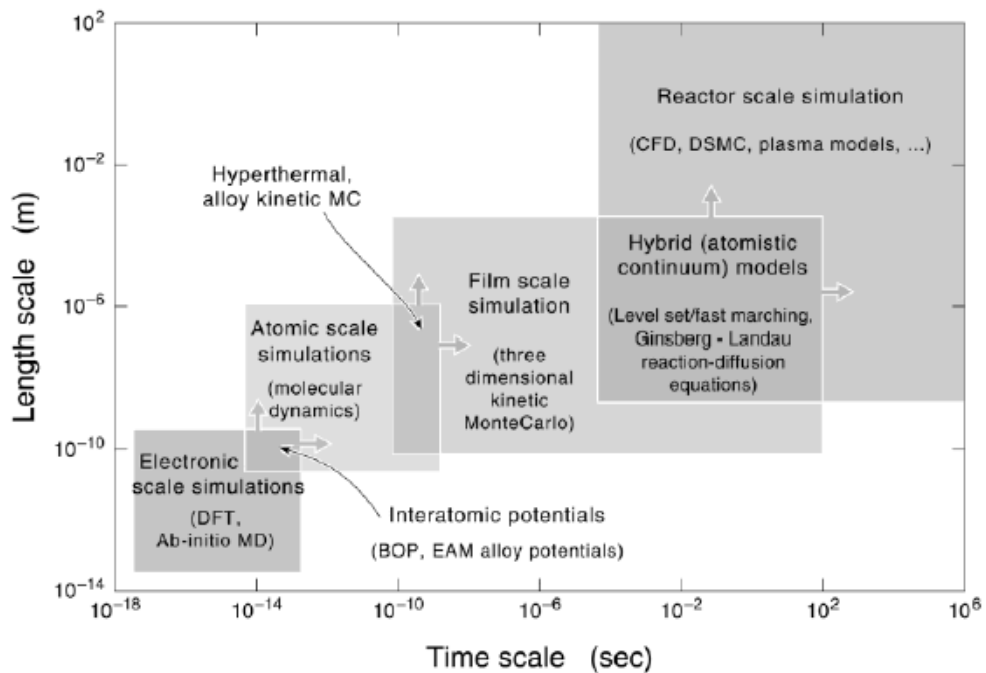


Fig. 1.2 The analysis of vapor deposition spans both a wide length and time scale. Overlapping modeling methods are beginning to allow an increasingly rigorous multiscale treatment [Ohno et al., 1999; Olson, 1997].

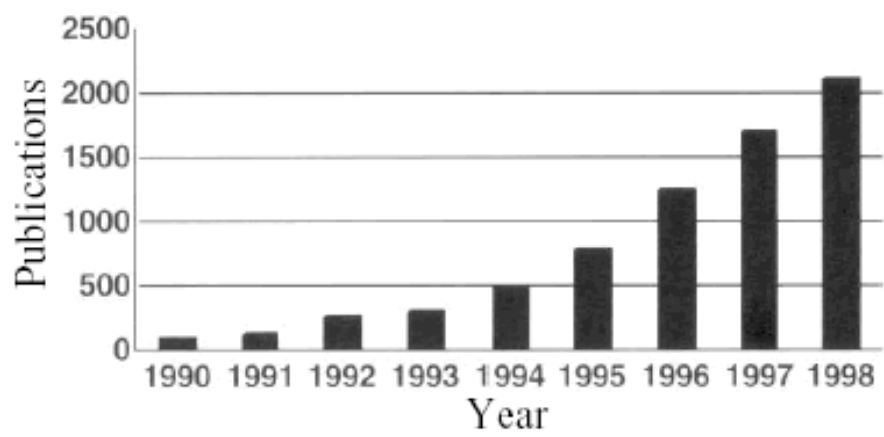


Fig. 1.3 The publications about DFT [Friedrich].

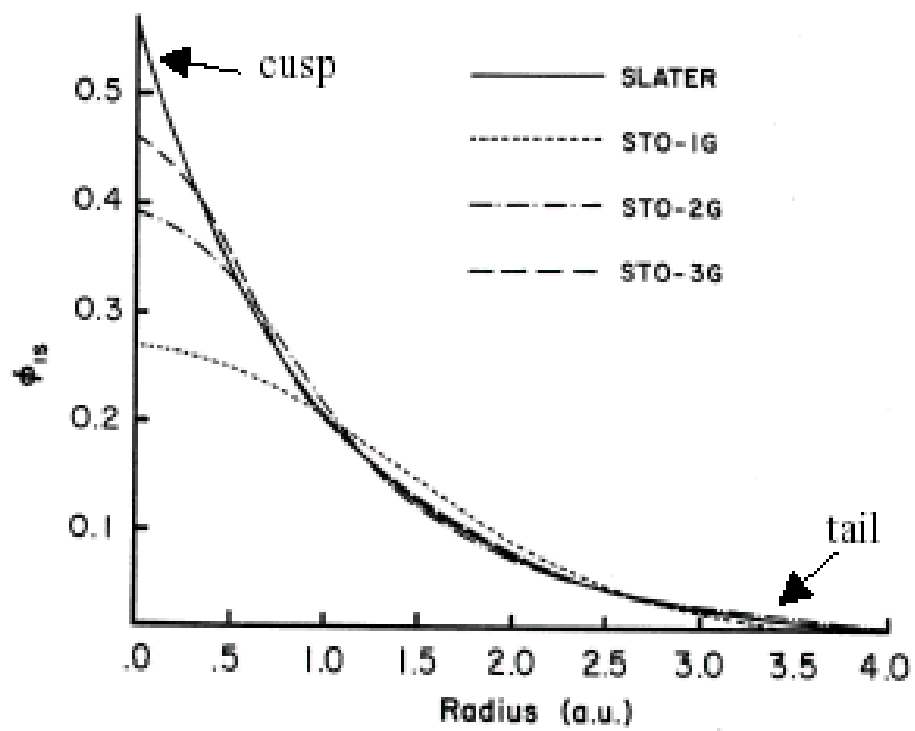


Fig. 1.4 STOs & GTOs [Friedrich]

I. EXACT GENERAL FORMULATION

1. The Density as Basic Variable

We shall be considering a collection of an arbitrary number of electrons, enclosed in a large box and moving under the influence of an external potential $v(\mathbf{r})$ and the mutual Coulomb repulsion. The Hamiltonian has the form

$$H = T + V + U, \quad (1)$$

where¹⁰

$$T = \frac{1}{2} \int \nabla \psi^*(\mathbf{r}) \nabla \psi(\mathbf{r}) d\mathbf{r}, \quad (2)$$

$$V = \int v(\mathbf{r}) \psi^*(\mathbf{r}) \psi(\mathbf{r}) d\mathbf{r}, \quad (3)$$

$$U = \frac{1}{2} \int \frac{1}{|\mathbf{r} - \mathbf{r}'|} \psi^*(\mathbf{r}) \psi^*(\mathbf{r}') \psi(\mathbf{r}) \psi(\mathbf{r}') d\mathbf{r} d\mathbf{r}'. \quad (4)$$

We shall in all that follows assume for simplicity that we are only dealing with situations in which the ground state is nondegenerate. We denote the electronic density in the ground state Ψ by

$$n(\mathbf{r}) = (\Psi, \psi^*(\mathbf{r}) \psi(\mathbf{r}) \Psi), \quad (5)$$

which is clearly a functional of $v(\mathbf{r})$.

We shall now show that conversely $v(\mathbf{r})$ is a unique functional of $n(\mathbf{r})$, apart from a trivial additive constant.

The proof proceeds by *reductio ad absurdum*. Assume that another potential $v'(\mathbf{r})$, with ground state Ψ' gives rise to the *same* density $n(\mathbf{r})$. Now clearly [unless $v'(\mathbf{r}) - v(\mathbf{r}) = \text{const}$] Ψ' cannot be equal to Ψ since they satisfy different Schrödinger equations. Hence, if we denote the Hamiltonian and ground-state energies associated with Ψ and Ψ' by H, H' and E, E' , we have by the minimal property of the ground state,

$$E' = (\Psi', H' \Psi') < (\Psi, H' \Psi) = (\Psi, (H + V' - V) \Psi),$$

so that

$$E' < E + \int [v'(\mathbf{r}) - v(\mathbf{r})] n(\mathbf{r}) d\mathbf{r}. \quad (6)$$

Interchanging primed and unprimed quantities, we find in exactly the same way that

$$E < E' + \int [v(\mathbf{r}) - v'(\mathbf{r})] n(\mathbf{r}) d\mathbf{r}. \quad (7)$$

Addition of (6) and (7) leads to the inconsistency

$$E + E' < E + E'. \quad (8)$$

Thus $v(\mathbf{r})$ is (to within a constant) a unique functional of $n(\mathbf{r})$; since, in turn, $v(\mathbf{r})$ fixes H we see that the full many-particle ground state is a unique functional of $n(\mathbf{r})$.

from P. Hohenberg, W. Kohn, *Phys. Rev.* 136, B 864 (1964)

Fig. 2.1 The proof of Hohenberg & Kohn second theorem

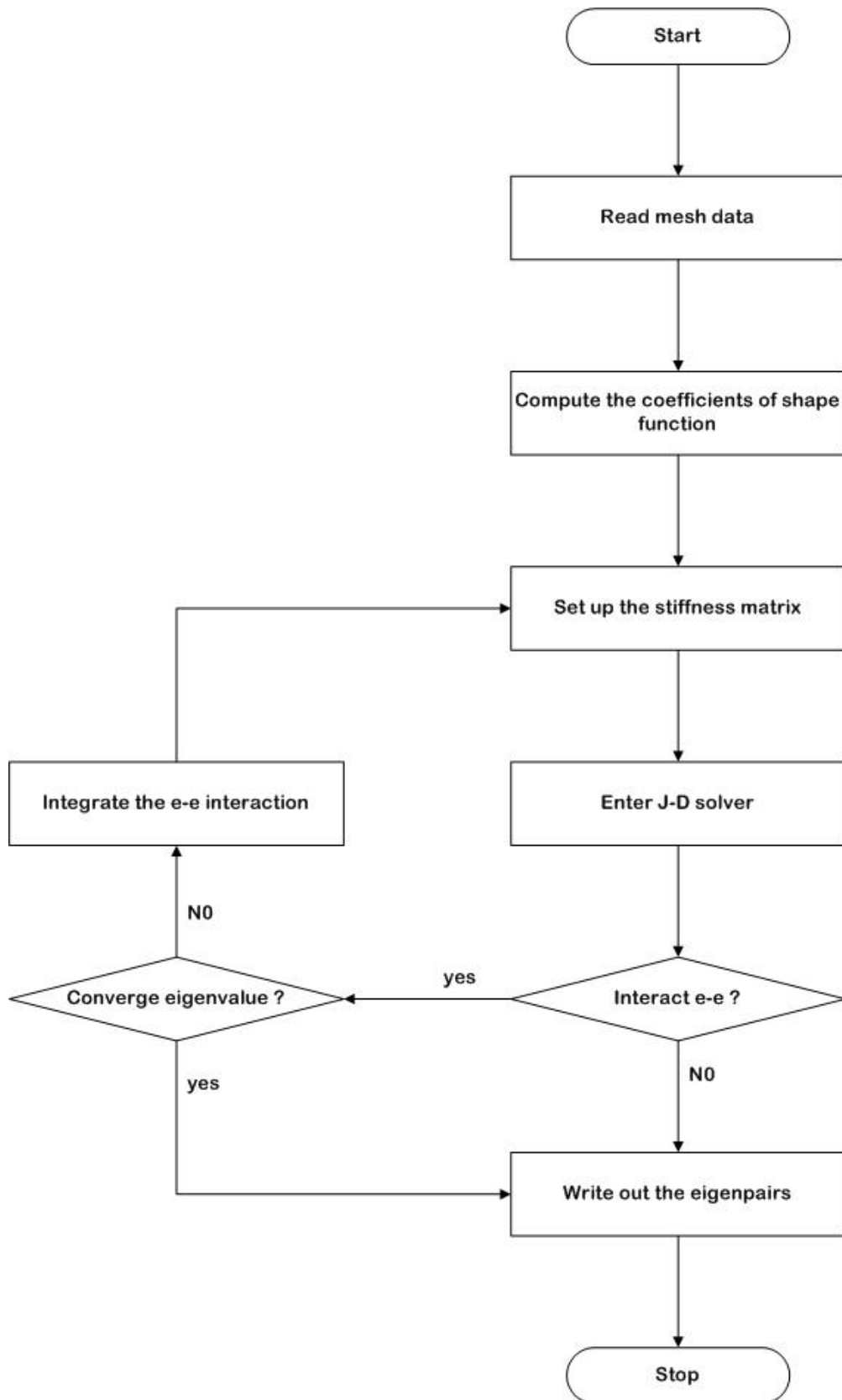


Fig. 3.1 The flow chart of the FEDFT.

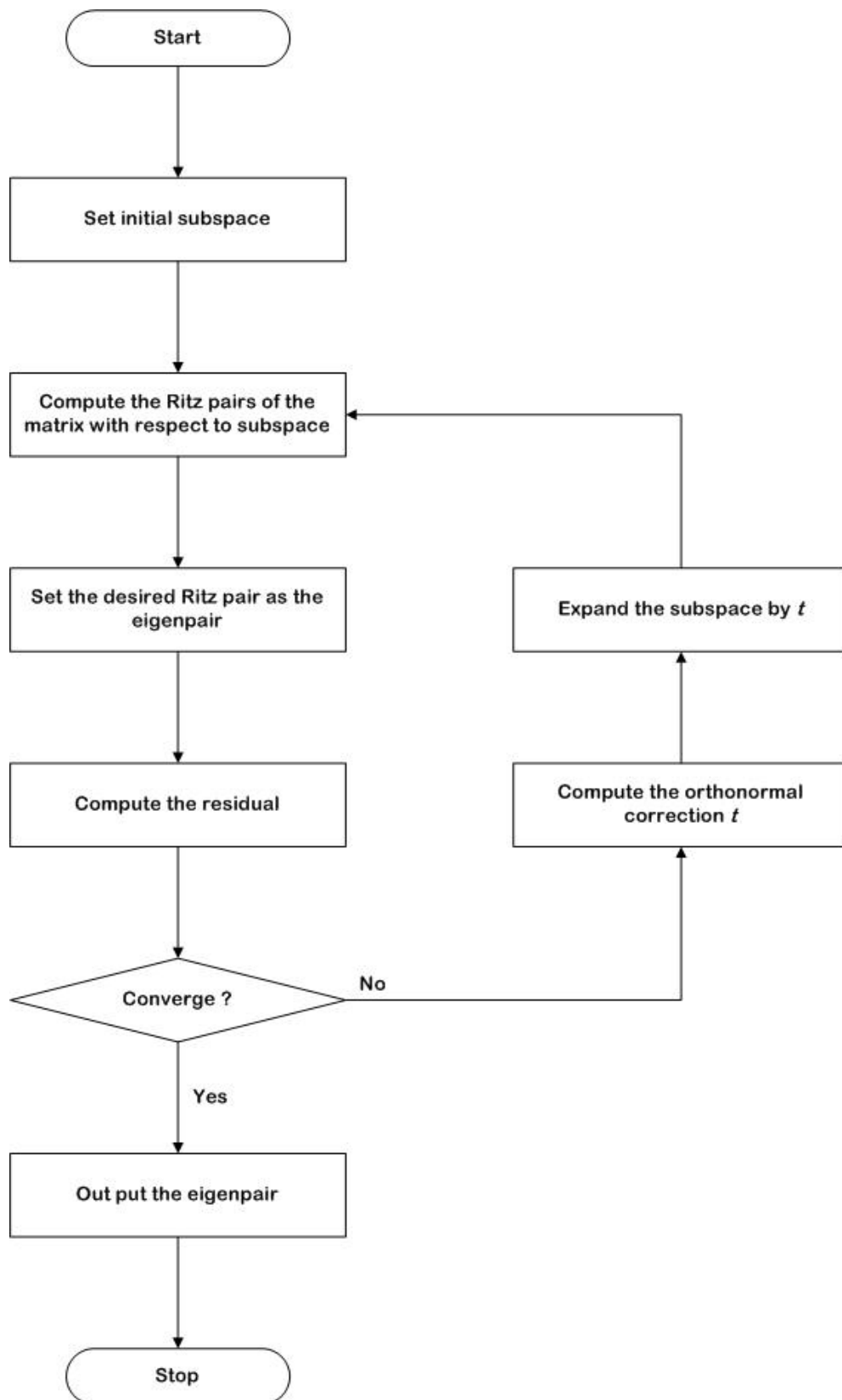


Fig. 3.2 The flow chart of the J-D solver.

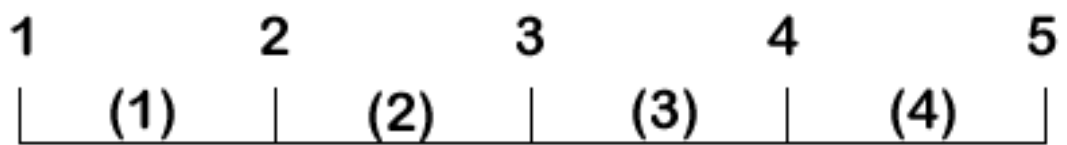
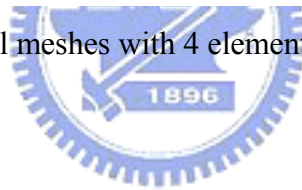


Fig. 4.1 One-dimensional meshes with 4 elements and 5 nodes.



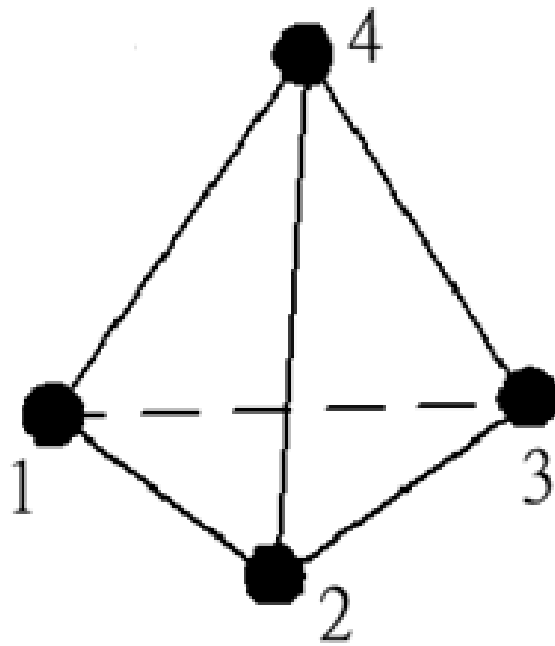


Fig. 4.2 The tetrahedral element.

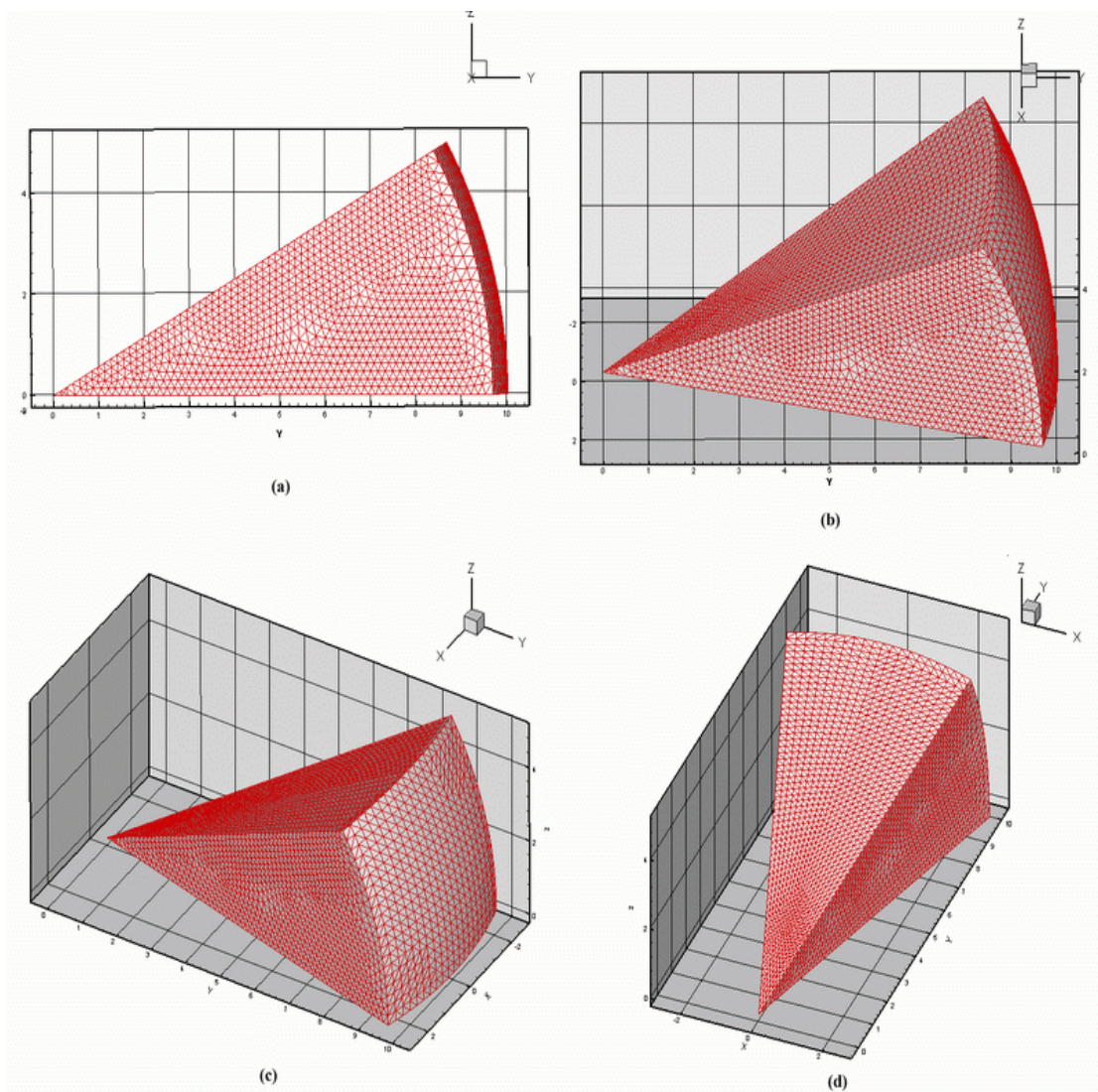


Fig. 4.3 The surface meshes of three-dimensional computational domain with different view points. ($r=10$ Bohr radii, $\theta=30^\circ$, $\phi=30^\circ$)

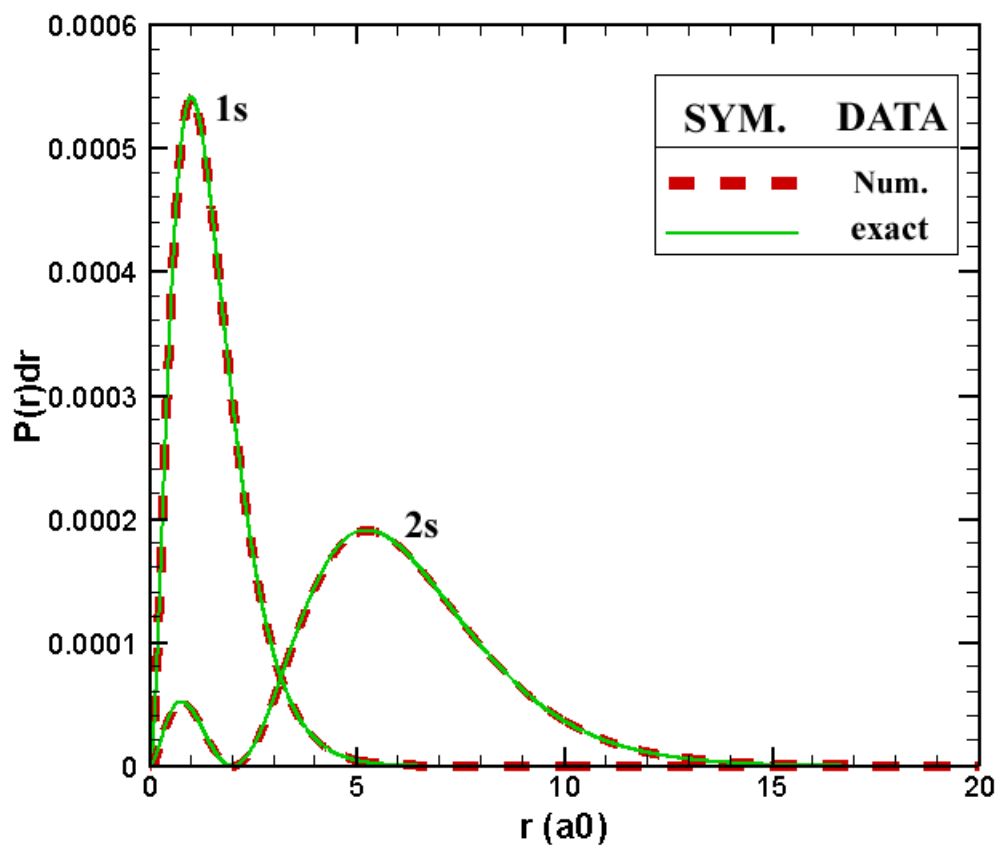


Fig. 4.4 The probabilities of finding the electron in a hydrogen atom at a distance between r and $r + dr$ from the nucleus for the 1s and 2s state obtained by one-dimensional FEDFT compared with exact solutions.

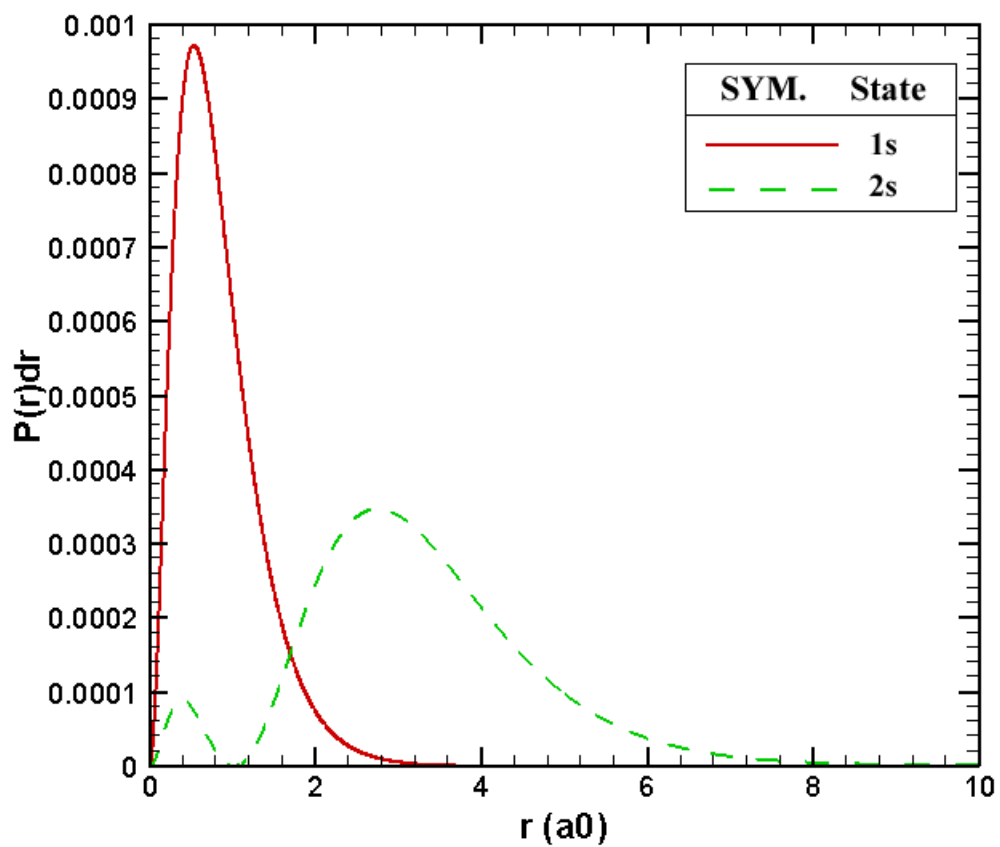


Fig. 4.5 The probabilities of finding the electron in a He at a distance between r and $r + dr$ from the nucleus for the 1s and 2s state obtained by one-dimensional FEDFT.

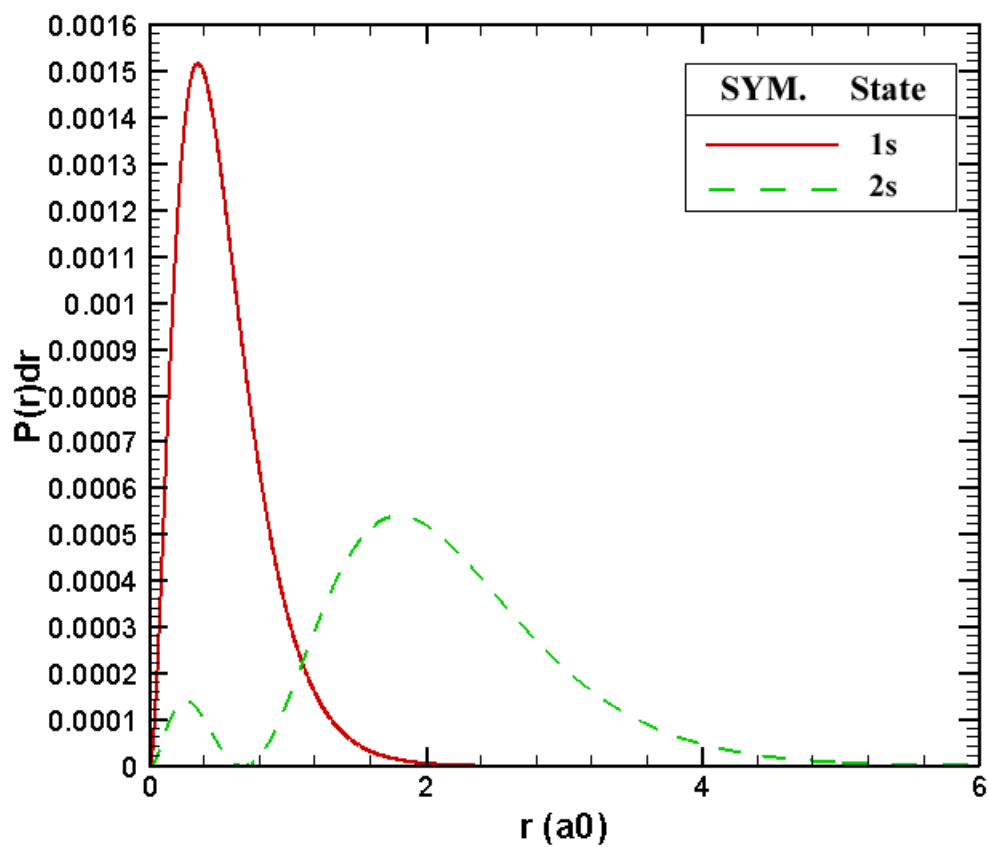


Fig. 4.6 The probabilities of finding the electron in a Li^+ at a distance between r and $r + dr$ from the nucleus for the 1s and 2s state obtained by one-dimensional FEDFT.

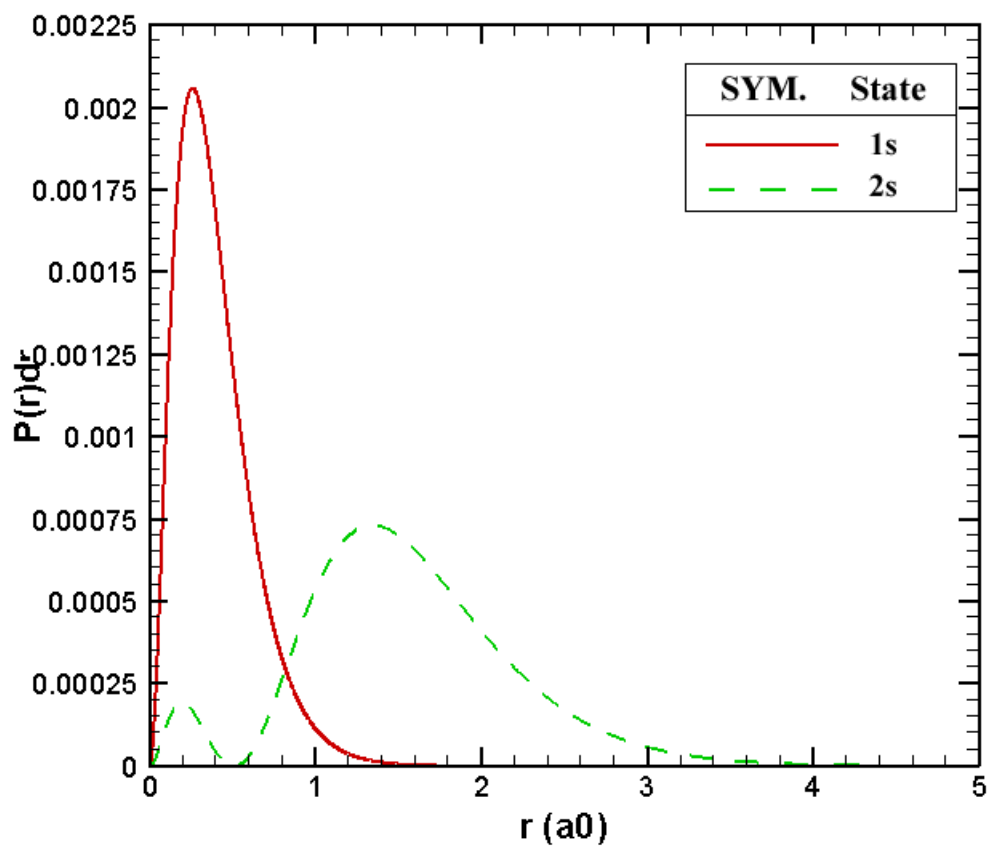


Fig. 4.7 The probabilities of finding the electron in a Be^{+2} at a distance between r and $r + dr$ from the nucleus for the 1s and 2s state obtained by one-dimensional FEDFT.

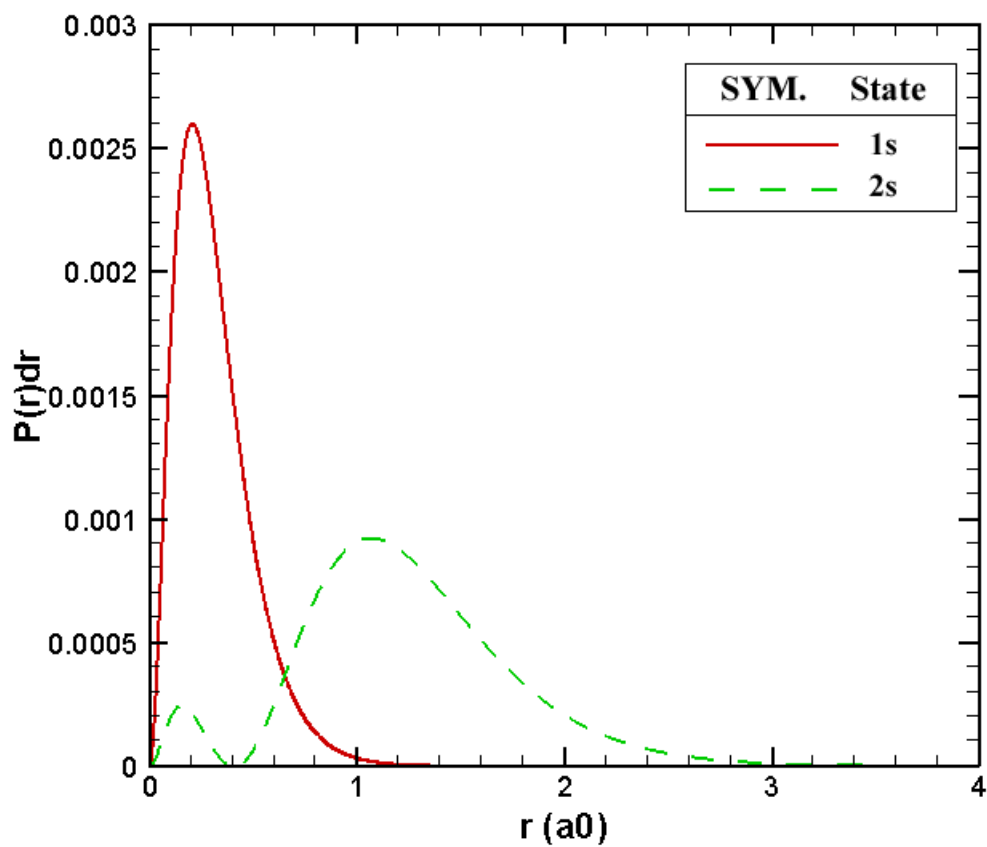


Fig. 4.8 The probabilities of finding the electron in a B^{+3} at a distance between r and $r + dr$ from the nucleus for the 1s and 2s state obtained by one-dimensional FEDFT.

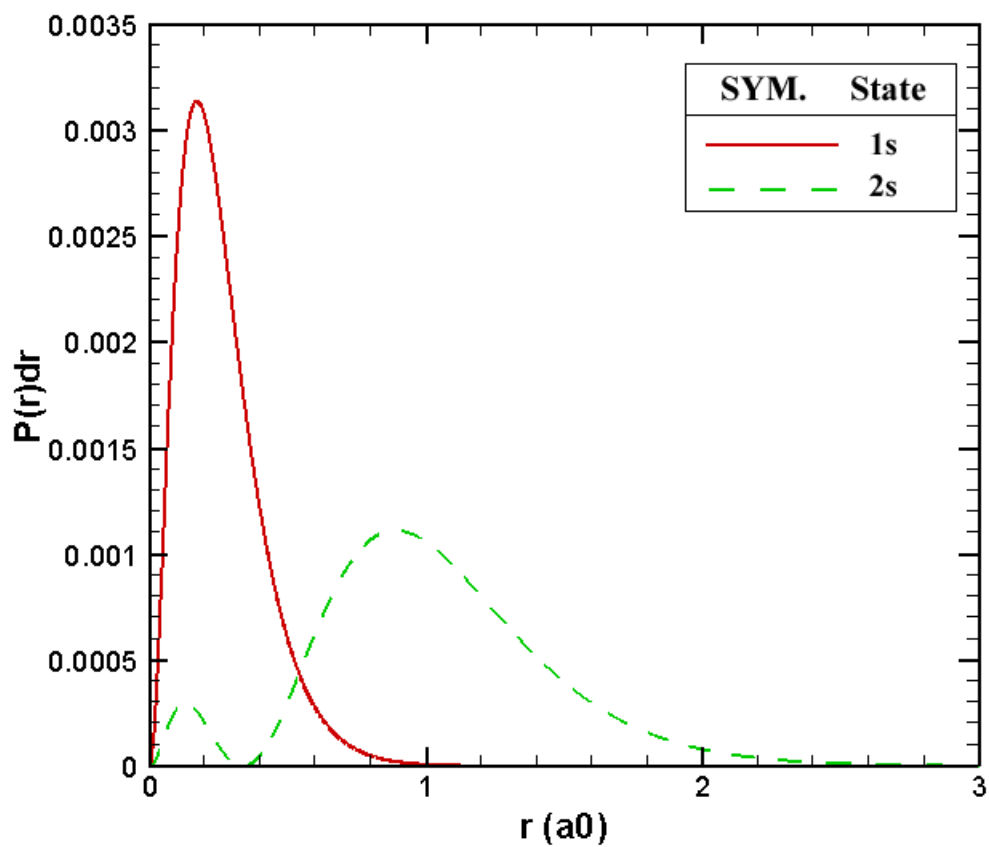


Fig. 4.9 The probabilities of finding the electron in a C^{+4} at a distance between r and $r + dr$ from the nucleus for the 1s and 2s state obtained by one-dimensional FEDFT.

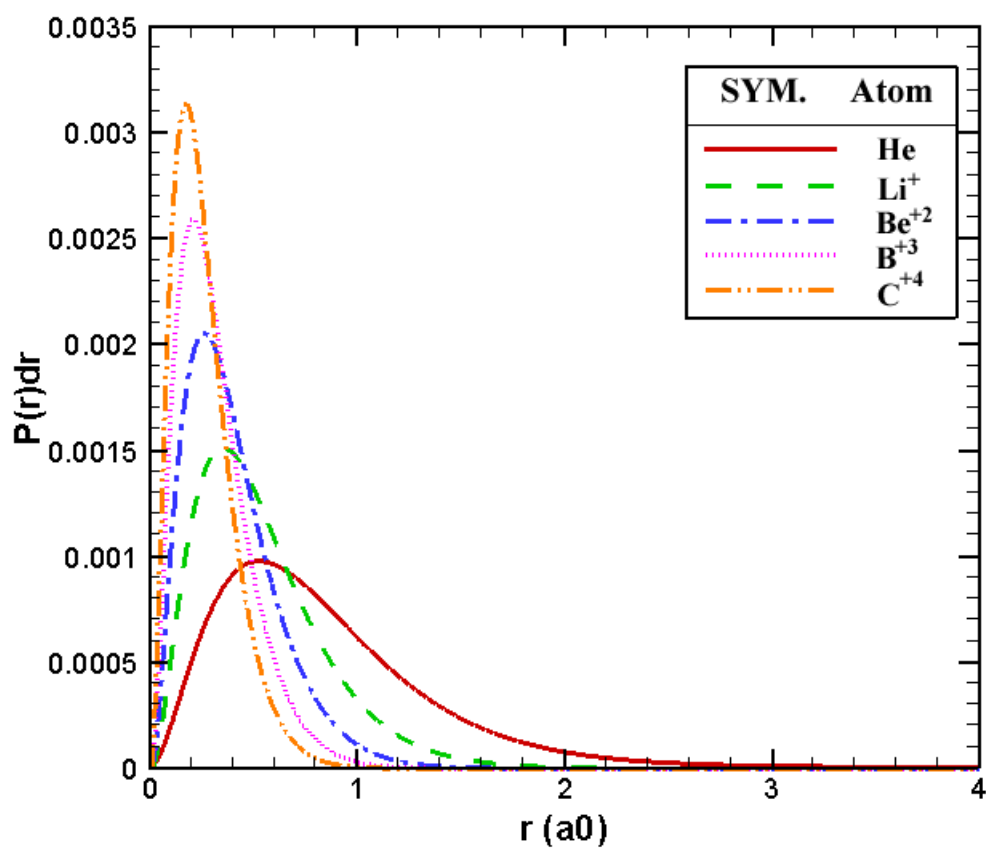


Fig. 4.10 The probabilities of finding the electron in helium-like atoms at a distance between r and $r + dr$ from the nucleus for the 1s state obtained by one-dimensional FEDFT.

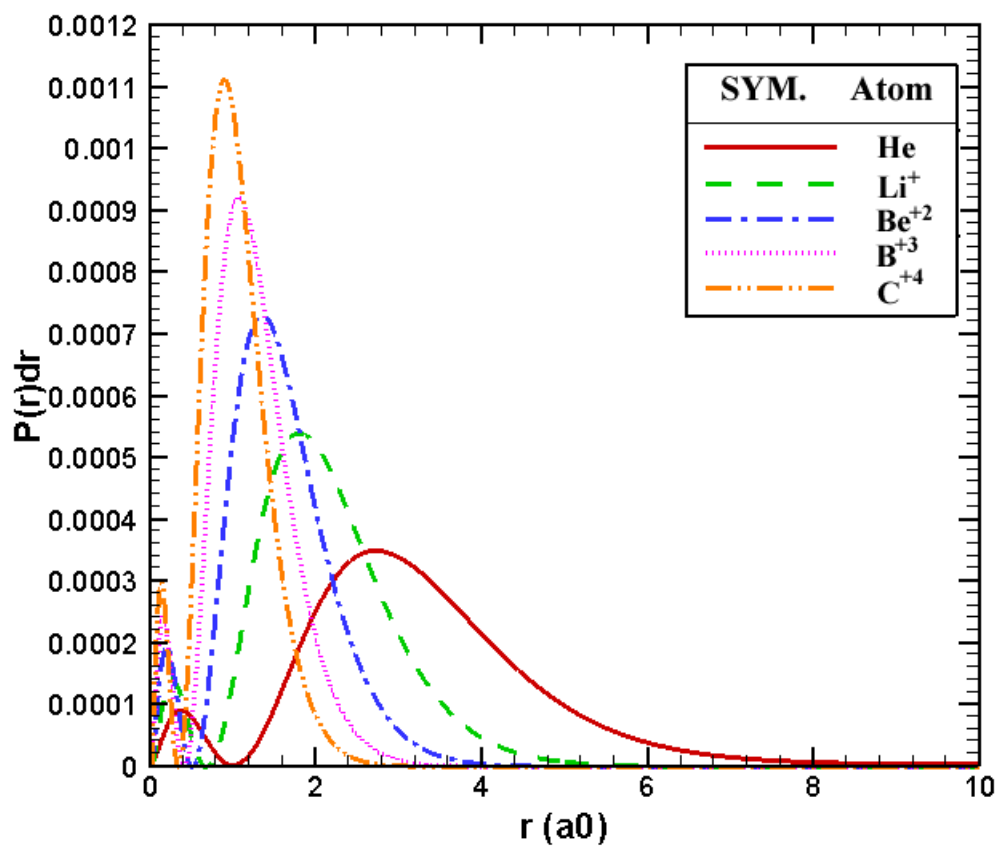


Fig. 4.11 The probabilities of finding the electron in helium-like atoms at a distance between r and $r + dr$ from the nucleus for the 2s state obtained by one-dimensional FEDFT.

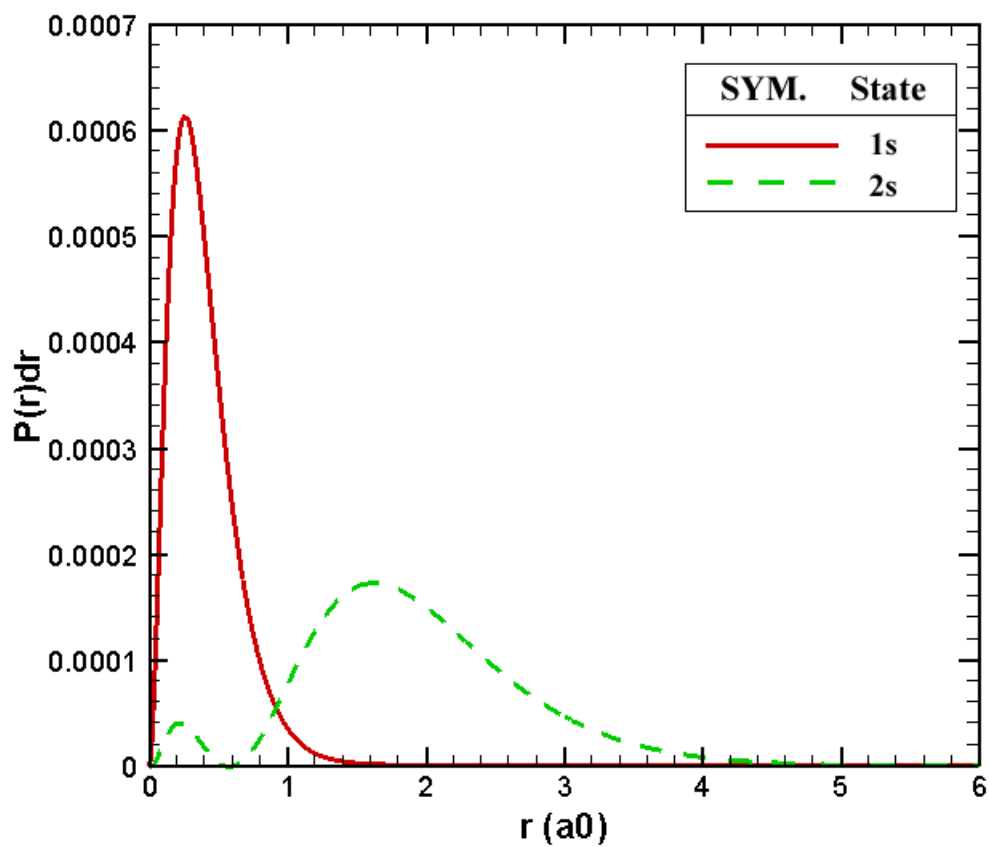


Fig. 4.12 The probabilities of finding the electron in a Be at a distance between r and $r + dr$ from the nucleus for the 1s and 2s state obtained by one-dimensional FEDFT.

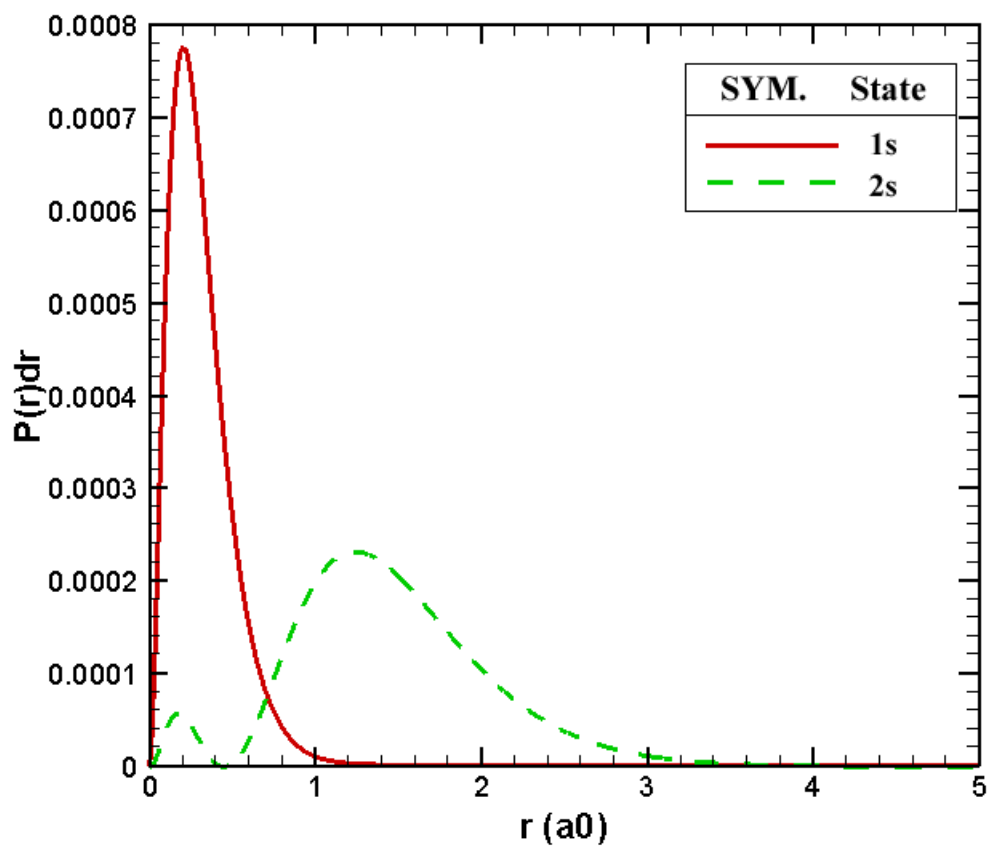


Fig. 4.13 The probabilities of finding the electron in a B^+ at a distance between r and $r + dr$ from the nucleus for the 1s and 2s state obtained by one-dimensional FEDFT.

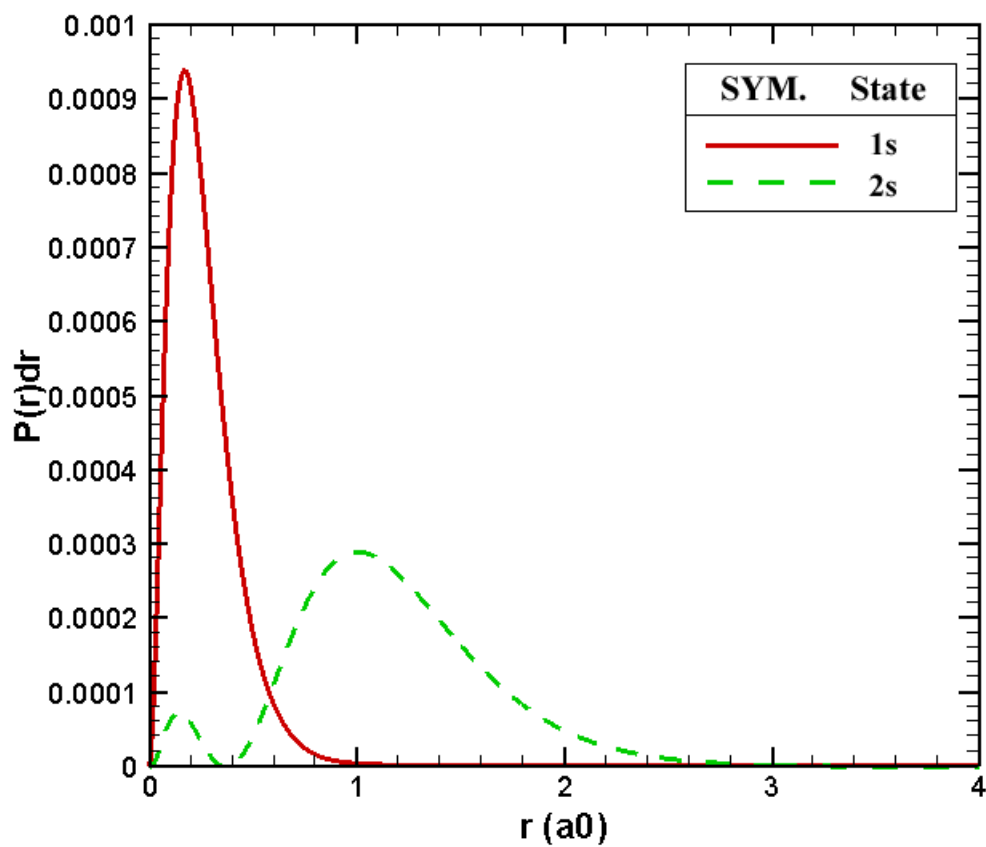


Fig. 4.14 The probabilities of finding the electron in a C^{+2} at a distance between r and $r + dr$ from the nucleus for the 1s and 2s state obtained by one-dimensional FEDFT.

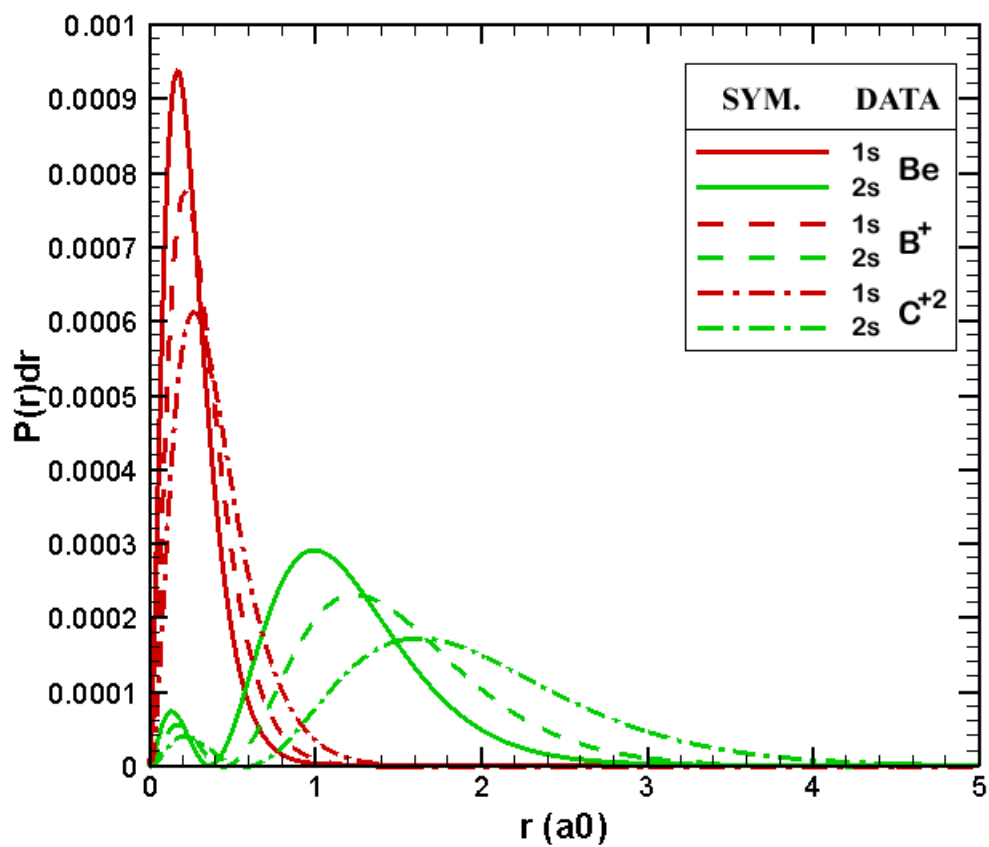


Fig. 4.15 The probabilities of finding the electron in beryllium-like atoms at a distance between r and $r + dr$ from the nucleus for the 1s and 2s state obtained by one-dimensional FEDFT.

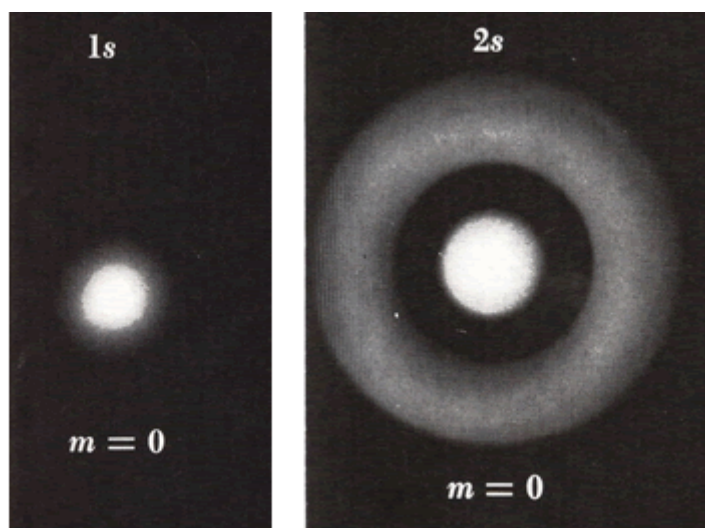


Fig. 4.16 Photographic representation of the electron probability-density distribution for 1s and 2s states. These may be regarded as sectional views of the distribution in a plane containing the polar axis, which is vertical and in the plane of the paper [Arthur, 1995].

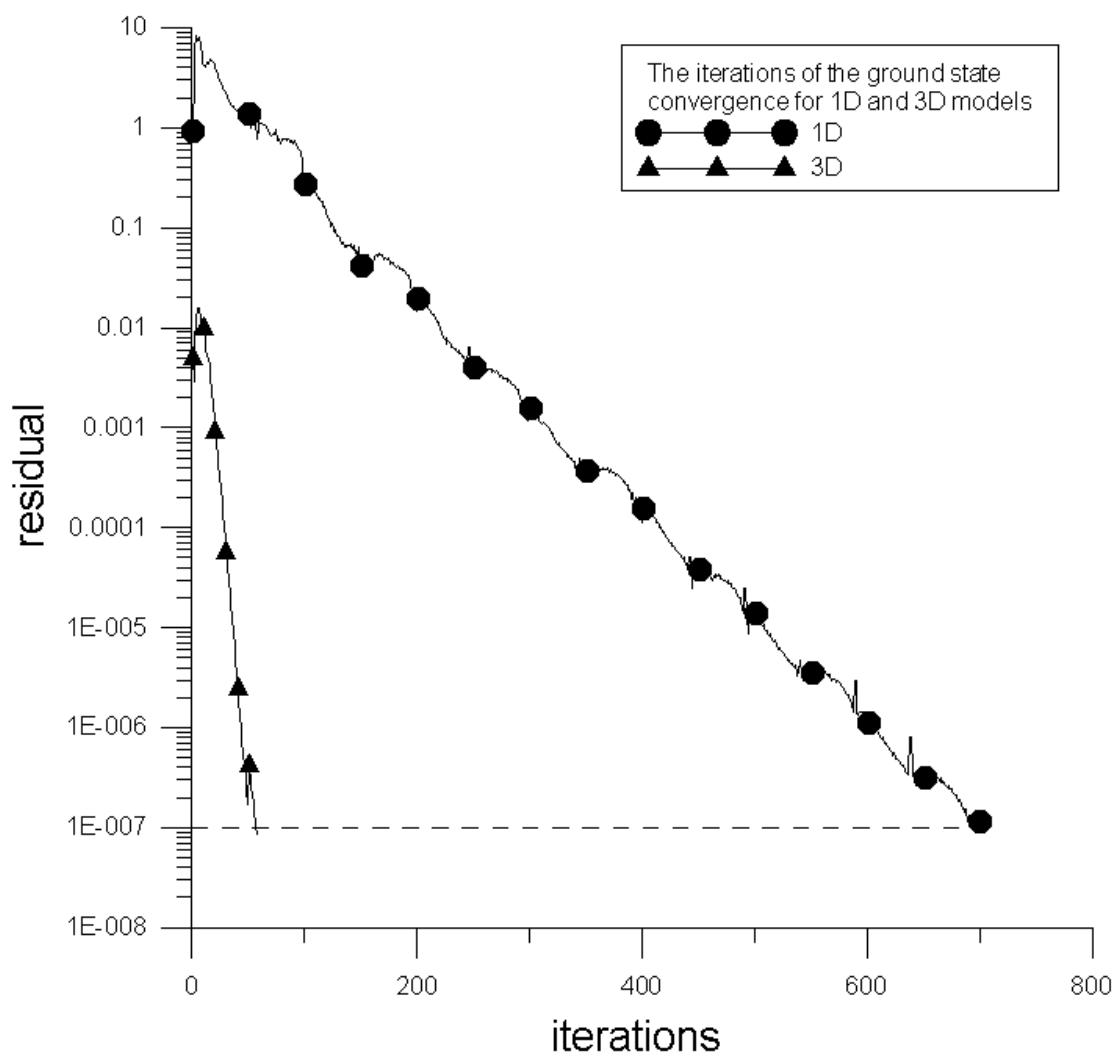


Fig. 4.17 The 1s state convergence of residual with iterations for hydrogen atom by one-dimensional and three-dimensional FEDFT.

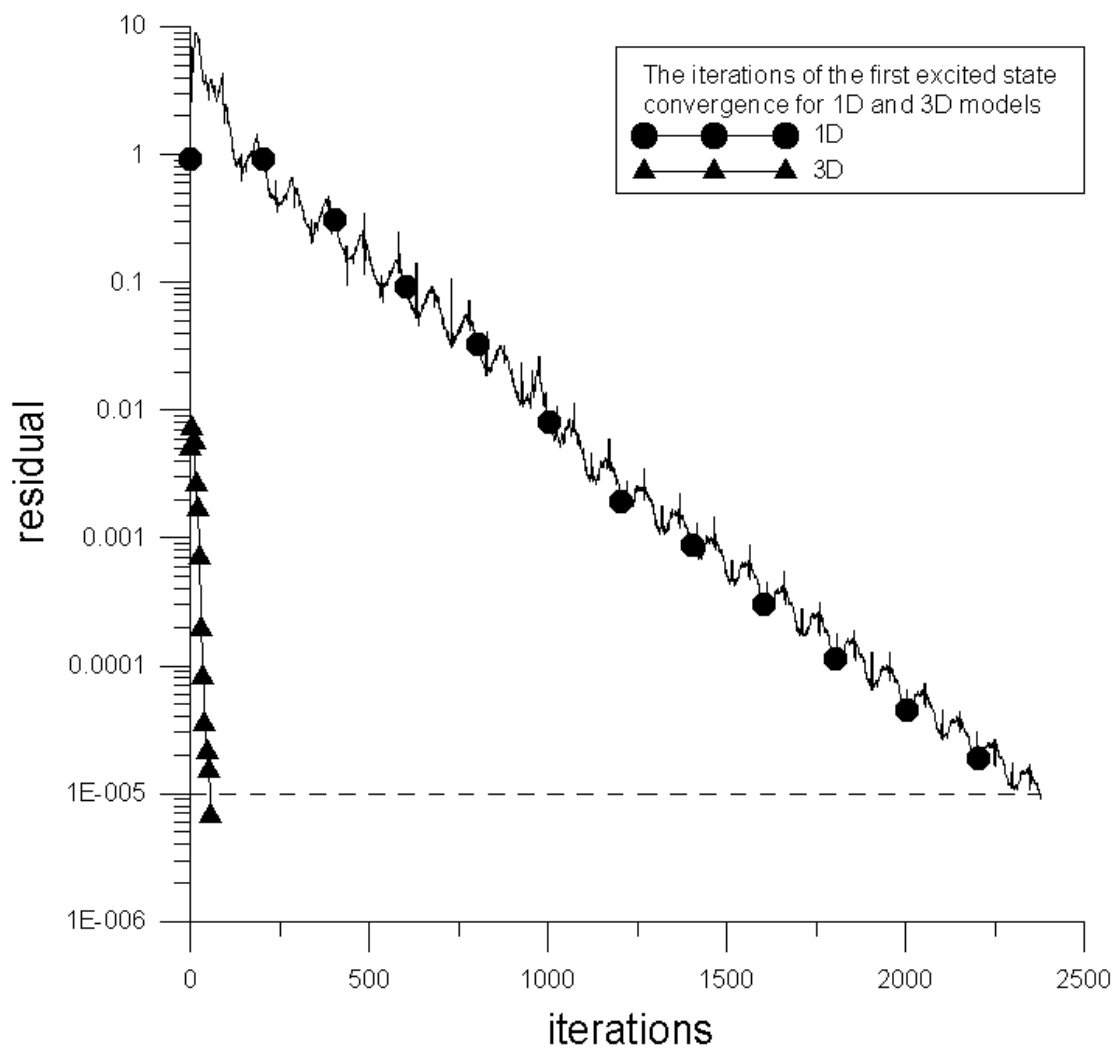


Fig. 4.18 The 2s state convergence of residual with iterations for hydrogen atom by one-dimensional and three-dimensional FEDFT.

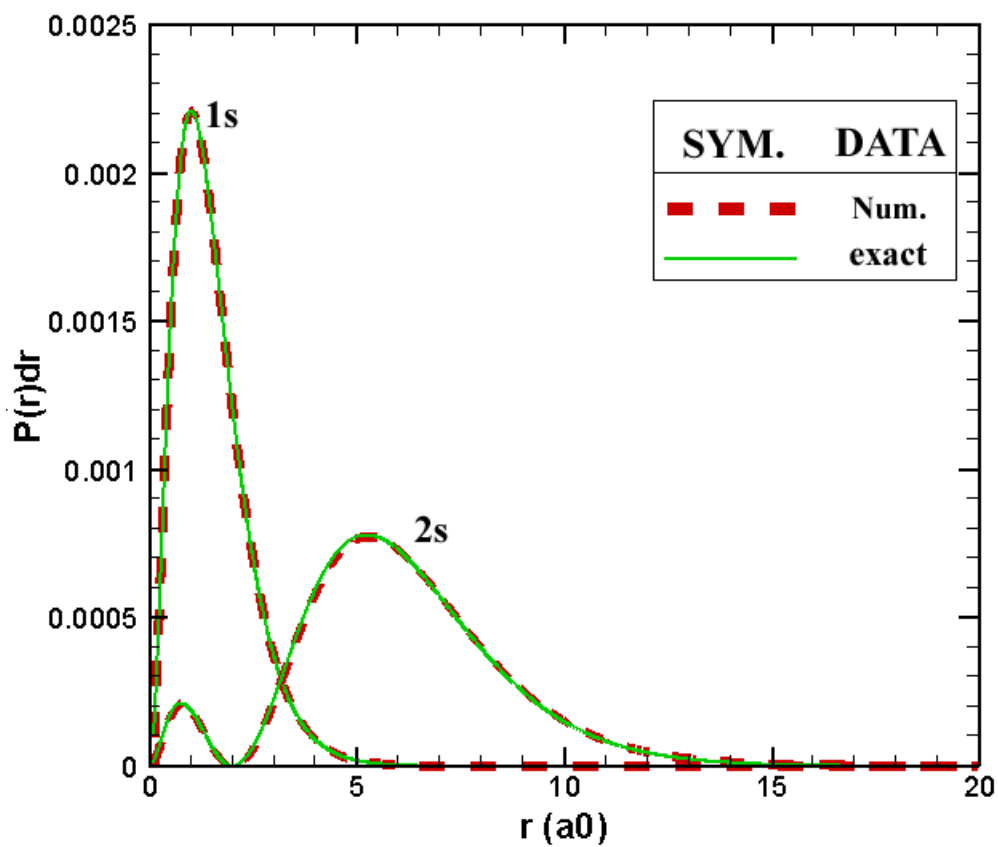


Fig. 4.19 The probabilities of finding the electron in a hydrogen atom at a distance between r and $r + dr$ from the nucleus for the 1s and 2s state obtained by three-dimensional FEDFT compared with exact solutions.

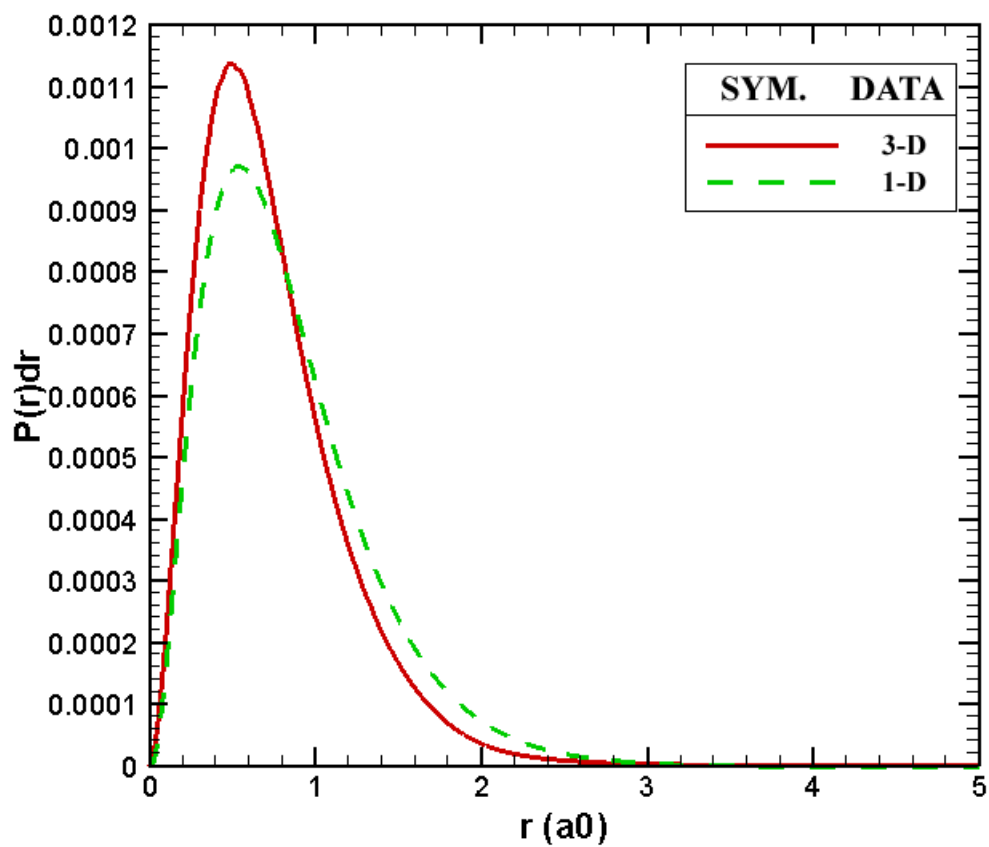


Fig. 4.20 The probability of finding the electron in a helium atom at a distance between r and $r + dr$ from the nucleus for the 1s state obtained by three-dimensional FEDFT compared with one-dimensional FEDFT.

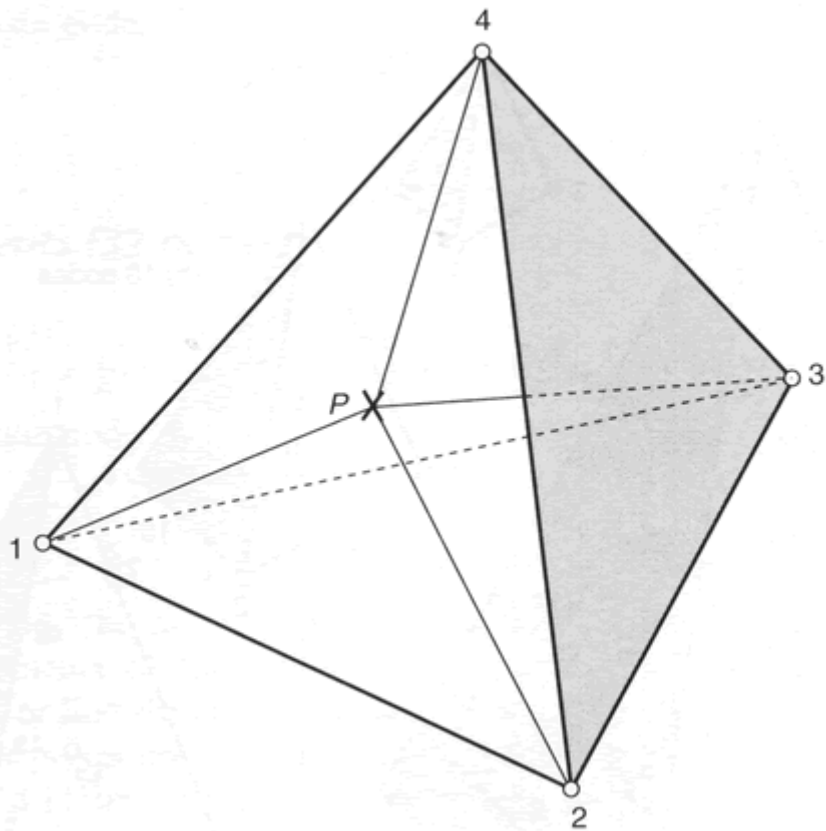


Fig. B.1 The coordinates of point P described by four edge nodes in the tetrahedral element [Zienkiewicz and Taylor, 2000].